Fabrication of a screen-printed electrode biosensor based on MoS_2/rGO functionalized electrode for uric acid sensing.

By

Hamza Yasin

School of Chemical and Material Engineering

National University of Sciences and Technology

2022

Fabrication of a screen-printed electrode biosensor based on MoS_2/rGO functionalized electrode for uric acid sensing.

Name: Hamza Yasin.

Reg. No: 00000277965

This thesis is submitted as partial fulfillment of the Requirements for the degree of

MS in Nanoscience and Engineering

Supervisor Name: Dr. Muhammaad Shoaib Butt

School of Chemical and Materials Engineering (SCME)

National University of Sciences and Technology (NUST)

H-12 Islamabad, Pakistan

Sep,2022

“With the greatest name of Allah Almighty,

Whose bounties are unbounded”

Dedication

This thesis is proudly dedicated to my parents:

Tariq Mehmood & Saeeda Tariq,

for their unconditional love, support, sacrifices, prayers, and advice.

Acknowledgments

First and foremost, praises and thanks to **ALLAH Almighty** for the blessings he bestowed upon me, gave me strength, good health, and the ability to learn and understand to complete this research successfully.

It is a genuine pleasure to express my sincere gratitude to my honorable supervisor **Dr. Muhammad Shoaib butt**, the best mentor, for sharing his experience and wealth of knowledge through his kind supervision, valuable guidance, and timely and constructive advice which helped me extensively in accomplishing my research work.

Besides my supervisor, I thank profusely my Guidance and Examination Committee (GEC) members **Dr. Sofia Akram, Dr. Mohsin Saleem**, **Dr. Irfan** and my fellow lab mates. I also acknowledge the help provided by fellows from the other labs especially **Muhammad Arman Liaqat**.

In addition, I would really love to give my sincere thanks to my best friend **Aqib Mehmood** for her ceaseless cooperation and support both in and outside the lab throughout my research.

Last but not the least, huge thanks to my beloved **Parents**, **Siblings,** and **My beloved family** for their unparalleled love, care, financial, encouragement, and emotional support, and lots of prayers.

Hamza Yasin

Abstract

A screen-printed electrode was fabricated with a nanostructure composed of Molybdenum Disulphide and reduced Graphene Oxide (MoS_2/rGO). The composites were prepared on MoS_2/rGO through a hydrothermal method. Scanning electron microscopy test tell us that nanocomposite has a flower-like shape, porous and large-surface region, X-rays diffraction (XRD), FTIR, Combining the properties of large surface region and exceptional electrical conductivity of MoS_2/rGO with the high electron affinity and specificity of biosensor, a smart progressively self-assembled electrochemical biosensor was established. The electrochemical performance was investigated by cyclic voltammetry (CV) at different molar concentrations of UA. The MoS_2/rGO sensor exhibits extraordinary electrocatalytic activity for detection of Uric acid (UA). A calibration plot with a coefficient of correlation of 0.9988 can be utilized to determine the linear connection between the current and UA concentration. The MoS_2/rGO@screen printed cupper-based electrode electrochemical sensor showed a sensitivity of 1.03 $mAmM^{-1}$ and limit of Detection (LOD) of 0.07mM (S/N = 3)**.** Furthermore, MoS_2/rGO nanocomposite shown strong performance for the detection of UA in samples, indicating that the suggested technique may be trustworthy and efficient for UA sensing in actual samples.

Table of Contents

.

List of Figures

List of Tables

List of Abbreviations

MoS_2	Molybdenum Disulfide.
RGO	Reduced Graphene Oxide
UA	Uric Acid
ES	Electrochemical Sensor
GO	Graphene Oxide
TMDs	Transition Metal Dichalcogenides
SPE	Screen Printed Electrode
XRD	X-rays Diffraction
SEM	Scanning Electron Microscope
FTIR	Fourier Transform Infrared Spectroscopy
CV	Cyclic Voltammetry

Chapter 1

Introduction

1.1 Introduction of Sensors:

A sensor is a device or gadget that detects particular analyses or substance and transmits it as a signal to a measuring or control instrument. Sensors are mainly designed to detect and respond to an analysis in the solid, liquid, or gaseous state. On the basis of response to be detected, sensors are broadly classified as chemical and physical sensors. Physical sensors would detect physical responses such as mass, temperature, strain, pressure, etc while as; chemical sensors have a chemical reaction or molecular analysis to be measured.

Uric acid (UA) is considered a pivotal little biomolecule in the physiological processes of the human digestion system. UA is the essential conclusion object of the purine digestion system, abnormal stages of which in purine and serum were an illustration of numerous maladies including hyperuricemia, pneumonia, gout and Lesch-Nyhan syndrome. In human physiological fluids AA, DA, and UA usually co-exist. The simultaneous determination of those three tiny biomolecules could be difficult trouble in terms of expectation and prevention of various infections. As a result, for measuring UA levels within the human body it is critical to develop a simple, facile highly selective, cost-effective, and sensitive approach. Different techniques are being utilized for the determination of Uric Acid as such like calorimetric fluorescence, chemiluminescence, and HPLC etc.

The best methods for detecting UA are electrochemical techniques because of their high sensitivity, ease of use, low cost, and quick examination period. Therefore, these species can be oxidized almost at the same potential as the conventional electrodes, and they almost cause electrode spots. At the modified electrode, different oxidation potentials and sensitive current responsiveness were attained, it is necessary to solve technological issues for electrochemical simultaneous assurance.

However, the biological compounds especially ascorbic acid (AA), glucose (Glu), and Dopamine (DA) co-existing with UA have comparable oxidation and reduction potential possibilities during the electrochemical detection. A variety of materials have been created and applied to change the working electrode making the detecting surface specific to UA, to overcome this difficulty.

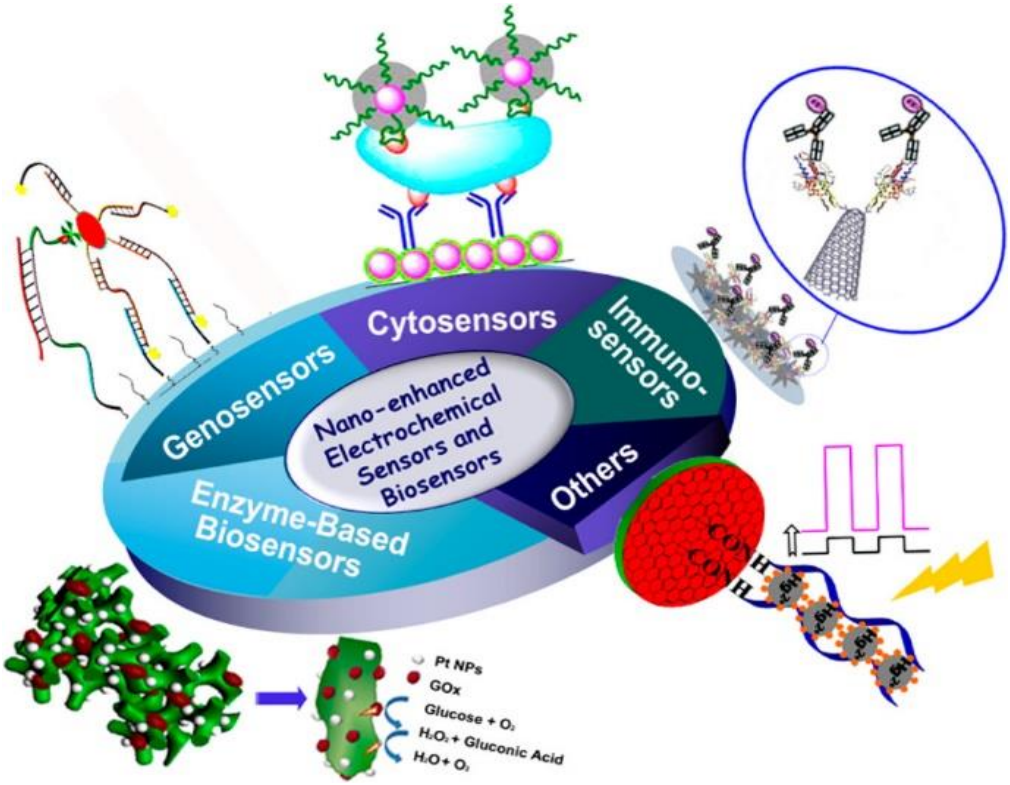

Figure1.1 Schematic of Electrochemical sensors

Graphene is viewed as a potentially disruptive material in a variety of recent advancements, including organic, power generation and storage, and optical applications, among two dimensional (2D) layered materials.

By stacking of sulfur-transition metal–sulfur sheets using TMDS graphene are formed. As a result, from majority material to mono-layer frames individual layers can be exfoliated. TMDS are expected to include Molybdenum disulfide (MoS_2). Mo atoms are stacked in hexagonal layers between two layers of S atoms in this material, which exhibits poor electric conductivity and p-type semiconducting characteristics. MoS_2 has two benefits in electrochemical (bio)sensors. First off, it offers more active sites that are electrochemically dynamic. Second one is that by adding other elements consisting of metal nanoparticles or bio recognition. It can improve transducer

properties. **[1]** However, there are a number of drawbacks to 2D MOS2, including the fact that restacking 2D diminishes the overall number of electrochemically active sites and their limited ability to operate as a transduction enhancer due to their lack of electrical conductivity. Therefore, combining 2D and MoS2 with additional conductive material, like graphene can help it overcome limitations and create compounds with intriguing properties.

Graphene a two-dimensional (2D) layered substance, has the ability to reverse many recent technological progress, including those in the fields of biology, energy storage, generation, and optics. **[2]** Having no dangling connections, the thinnest (atomically thin) unsupported crystalline solid that allows for significant intralayer transmission of light, spin, and charge are 2D layered materials. **[3]** The potential for graphene to stand out among the 2D layered materials comes from its single layer of carbon molecules bound in a hexadic honeycomb web. **[4]** There are various benefits to employing graphene-based materials in electrochemical transducers due to the ultra-thin nature of graphene, such as enhanced conductivity, electron exchange rate, or transducer surface-to-volume ratio. **[5]** Another crucial aspect of this special Graphene substance is its ability to be functionalized with heteroatoms, molecules, or other atoms.

The presence of oxygen functional groups has a significant impact on the electrical and chemical characteristics of graphene-based materials. Reduced graphene oxide (rGO) and Graphene oxide(GO) are frequently employed in biosensors and bioelectronics due to their hydrophilicity (than graphene) and close proximity to oxygen-containing groups. It's worth noting that the conductivity of graphene decreases as the amount of oxygen-like substance increases, necessitating the use of a material with a precise C/O ratio for specific purposes.

MoS_2 or a combination of TMDs have been used in a number of documented demonstrations of electrochemical Biosensors. **[6]** However here we concentrate on graphene-based composite containing materials MoS_2 (Gr/ MoS_2). In this, rGO/ MoS_2 nanocomposite with porous or fragile nanostructure, massive particular surface area, and great electrical conductivity transformed into an organized one-pot hydrothermal process. The electrode material of the rGO/ MoS_2 nanocomposite, which combines rGO and MoS_2, is used to efficiently produce a stable, reproducible, and selective electrochemical biosensor for simultaneous detection of Uric Acid.

1.2 Sensors in Different field

1.2.1 Sensors for detection of lead ions in tobacco leaves:

In order to increase sensor sensitivity for the electrochemical measurement of heavy metals, high-performance electrode modification materials are essential. In the work, a modified glassy carbon electrode (GCE) consisting of MoS_2/rGO/CS nanocomposite was utilized to made an effective sensor for detection of Pb(II) ions in tobacco leaf. Reduced graphene oxide (rGO) was employed to increase the conductivity of the sensor, and nanoflowered MoS2 was able to provide a sizable quantity of collective response surface area and a new active region for heavy metal reaction. Chitosan was used to improve the electrocatalytic activity of the electrode and the ability of heavy metal ions to be enriched. Thus, a reproducible stable and excellent performing electrochemical sensor with good anti-interference capabilities was constructed.

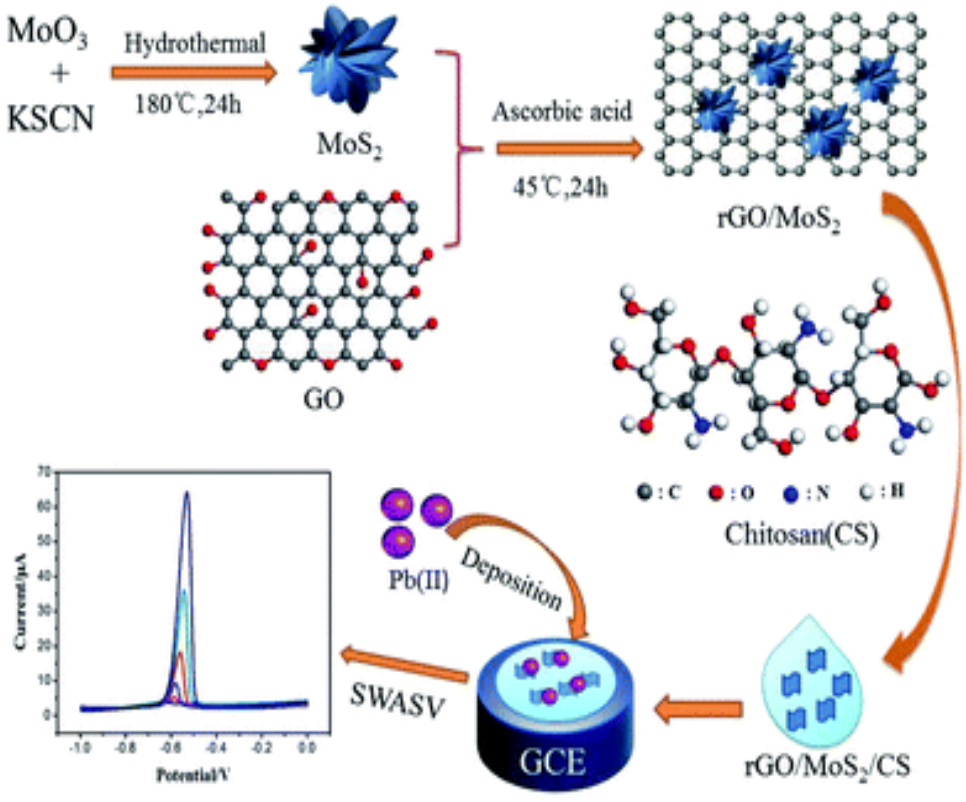

Figure 1.2 A Schematic showing the electrochemical analysis procedure for Pb(II) and the developed sensor based on GCE modified with rGO/MoS2/CS.

1.2.2 Sensors for detection of Nitrogen Dioxide at room temperature

To detect nitrogen dioxide (NO2) gas at a parts per billions grade (ppb) at ambient temperature, chemically resistive sensors have been developed. These sensors use binary and ternary hybrids of reduced graphene oxide (rGO). The sensors base hierarchical structures of MoS_2 sheets coated with rGO and sub-subsequent integration with silver nanoparticles(AgNPs) have better sensors responses and lower detection limits than the unary counterpart (rGO). At a concentration of 1ppm, the ternary hybrid device/s sensing response increased by about 500% over rGO alone, and at a concentration of 104 ppm. In terms of sensitivity to NO_2, the ternary hybrid device performs better than the binary and the unary counterparts throughout a broad concentration range from1ppm to 104ppm. The ternary hybrid device is not only very selective to the air pollutants like ammonia, carbon monoxide and Sulphur dioxide.

1.2.3 Gas Sensors

The recent security situation in the area has not been understated. Preventing terrorist attacks acts of extremism, and significant emergencies in crucial. Defense against chemical weapon, countering biological terrorism, and dealing to chemical accident are the three main operational requirements of national defense. Therefore, it is crucial to quickly, and precisely detect poisonous, accurately and harmful gases. This paper lays the foundation for future research by reviewing the development of MoS_2/rGO nanomaterials in gas sensors.

Gas sensors have been the subject of extensive research MoS_2. However, its limited structural strength and poor electrical conductivity limit its viability as a raw material for gas sensors. The conductivity and physical strength shortcomings of intrinsic MoS_2 make it difficult to further expand its possible uses. The material's gas sensing performance is significantly enhanced by the layered by a layered composite structure made of rGO/MoS_2 nanomaterials. **(Figure1.3)** The resulting MoS2 composite containing graphene can be contained in the button cell using the cell fabrication process to evaluate its electrochemical properties. Some of the characterization techniques including galvanized charge-discharge testing, and cyclic voltammetry. Because both MoS_2 and graphene have high conductivities and increase the electronic properties of nanomaterials are superior to those of pure MoS_2 and graphene. Additionally, the porous nature of graphene can improve its capacity for storing lithium ions and facilitate in the diffusion of electrolytes. MoS_2 considerably

enhances the rate performance of materials and reduces the transmission distance of lithium ions. **[7]**

The findings of the electrochemical evaluation show that the special features of graphene can be successfully used, the complementing features of graphene and molybdenum disulphide may be obtained, the detailed features of composite can be greatly enhanced, as can the energy storage capability and durability of the nanocomposite, the effectiveness of graphene material for a practical implementation, the synergistic and the surface effect properties of the composite and the usefulness of graphene in general.

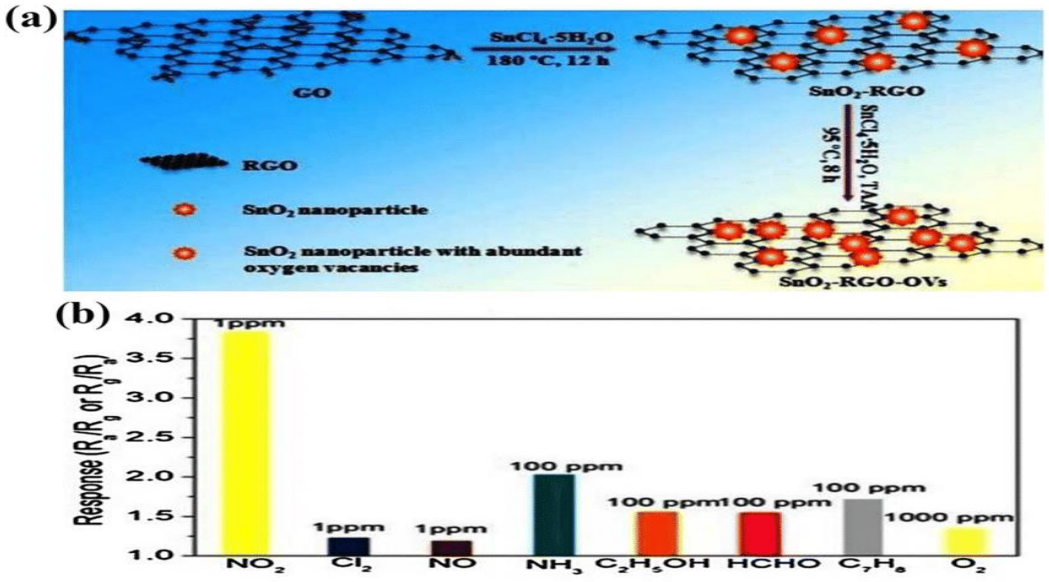

Figure1.3 Schematic diagram of the preparation of SnO_2/rGO/Ov nanocomposite. **[7]**

Application of Different materials in gas sensors

A typical hazardous gas that is strongly connected to people's daily lives is formaldehyde (HCHO). Many newly decorated rooms and recently purchased autos contain HCHO. Consequently, civil sensors research has long focused on the HCHO gas sensor. Materials called MoS_2/rGO were used by researchers to detect formaldehyde. MoS_2/rGO gas sensors were built on poly naphthalene dicarboxylate) vinyl using a straightforward and simple self-assembly technique, allowing for the creation of a flexible formaldehyde sensing element that operates at room temperature. The MoS2/rGO sensor can detect ppm formaldehyde and has a good sensitivity to it. according to the findings of the sensing experiments. Additionally, compared to pure reduced graphene oxide sensors, MoS_2 composite with rGO-based

sensors exhibit better sensitivity. This may be because two-dimensional materials' HCHO adsorption and electron transfer abilities have improved as a result of the MoS_2 composite. The procedure was used to create various MoS_2 nanosheets, and it was then used to compare how sensitive they were to HCHO. Results indicate that MoS_2 nanosheets made using the hydrothermal process have higher sensitivity and more flaws than those made using other methods, which increases the sensitivity of MoS_2/rGO-based sensors.

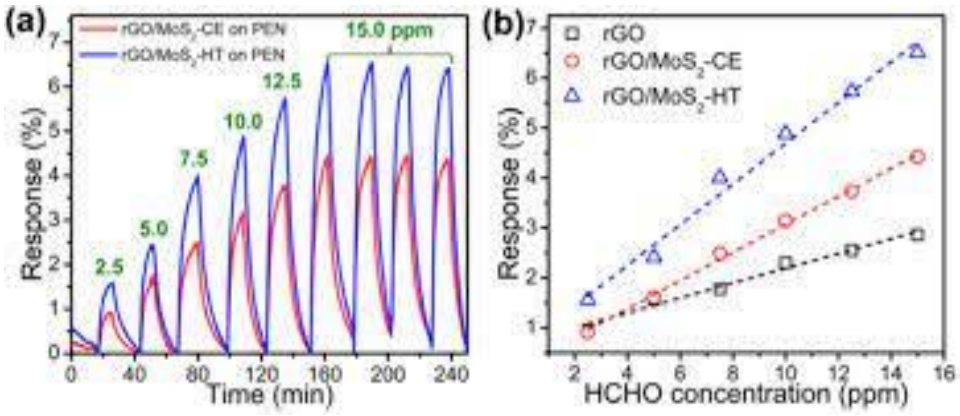

Figure1.4 Real-time detecting quantitative results of the rGO/MoS_2 and rGO/MoS_2-CE sensors to 2.5-15.0ppm HCHO are shown in Figures (a) and (b).

Numerous toxic gases are released into the atmosphere as a result of the chemical industry's rapid growth and the energy market's growing energy consumption. Nitrogen oxide (NO_x), ammonia (NH_3), hydrogen (H_2), and carbon monoxide are the most prevalent hazardous gases (CO). NO_2 and NH_3 are two of these dangerous gases that not only impact the environment but also people's health by causing pulmonary edoema, acid rain, and other health problems like ozone layer damage. By using a hydrothermal process, Neha Kanaujiya created MoS_2 that looked like petals before creating MoS_2 composite graphene materials.

1.2.4 Sensors for energy storage device

It is essential to develop adaptable, high-performance energy storage methods for power supplies given the quick development of wearable electronics. As smart energy sources for wearable technology, flexible fiber super-capacitors (FSCs), which can be woven into fabrics and have a high degree of flexibility, are gaining popularity. In recent years, FSCs composed of various electroactive materials have been developed, and when utilized to power wearable electronics with a variety of applications, they have shown outstanding electrochemical performance. Due to their low weight, small

volume, excellent conductivity, high mechanical strength, and knittability, carbon nanotube (CNT) fibers have been considered to be among the most appealing binder-free electrode materials for FSCs Pseudocapacitor materials like Conductive polymers and transition metal oxides/sulfides are frequently used as the coating layer to enhance the electrocatalytic activity of CNT fibers. Reversible redox reactions occur in this pseudocapacitor material, increasing the specific capacitance of the FSC.

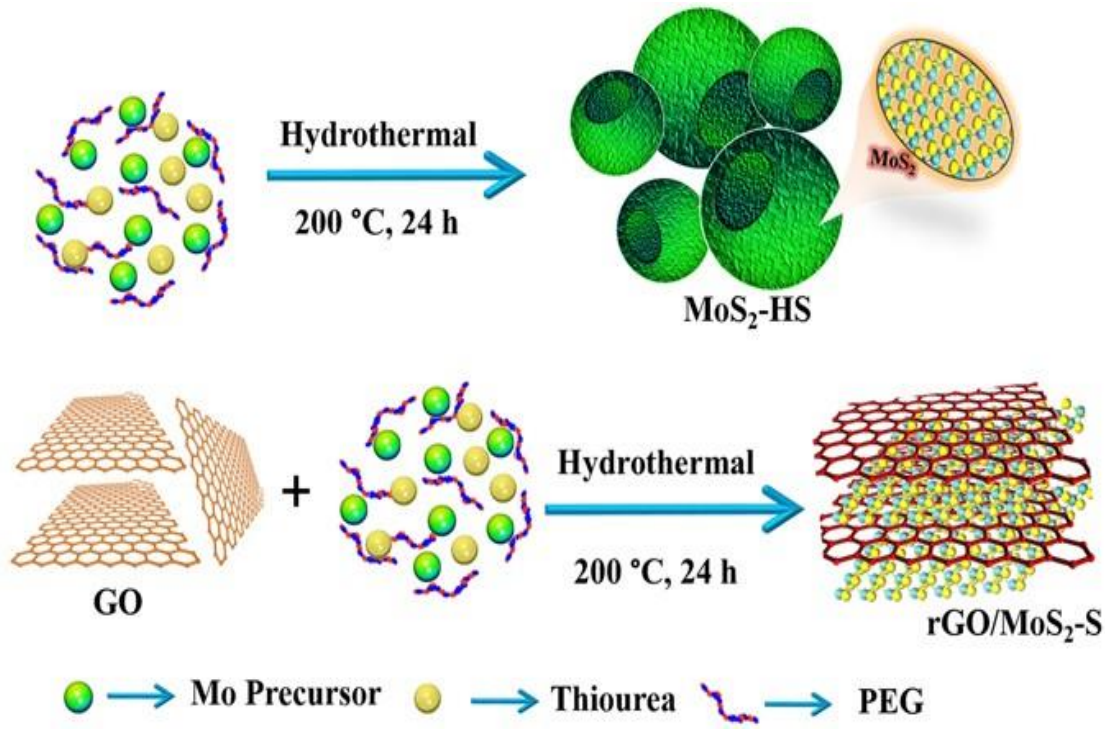

Figure1.5 Schematic of MoS_2/rGO for energy conversion and storage application

1.2.5 Sensors for detection of electrochemical Immunosensor (detector)

Humans now die from cancer more frequently than any other disease, and early cancer detection depends on finding cancer markers in human serum. Carcinoembryonic antigen (CEA), a proteoglycan complex, is frequently utilized as a diagnostic for the early identification of cancer and recurring malignancies. However, adult colon tissue only contains a very small amount of CEA about 2.4 μg L^{-1}. Thus, a variety of applications will be possible for high-sensitivity CEA diagnosis. Since label-free immunosensors are simple to work with and preserve protein activity, they are frequently utilized to detect cancer markers. Lung, Colorectal, gastric, breast, and pancreatic malignancies have all been treated using these immunosensors.

There are several techniques for CEA detection, including electrochemiluminescence

techniques, fluorescent immunoassays, and enzyme-linked immunosorbent assays. Electrochemical immunoassays are frequently employed due to their inherent benefits, high sensitivity, simplicity of apparatus, ease of miniaturization, low cost, and quick analysis. Particular focus has been placed on non-enzymatic immunosensors because to their excellent specificity and sensitivity. Carbon-based materials, metal oxides, and metal nanoparticles are just a few nanomaterials that have gained international interest.

Recently, it was shown that the material Molybdenum disulfide MoS_2, which resembles graphene, has the following properties: a large particular surface area, favorable electron transfer properties, high stability, energy band adjustment, ease of synthesis process, nontoxicity, and a high electrical conductivity, and chemical bonding. In the study of electrochemistry, chemical and physical properties have garnered a lot of interest. The issue is made more fascinating by the possibility that MoS_2 will operate as a solid support for the hybridized of organic compounds or inorganic materials. However, there are certain issues with MoS_2 in real-world applications.

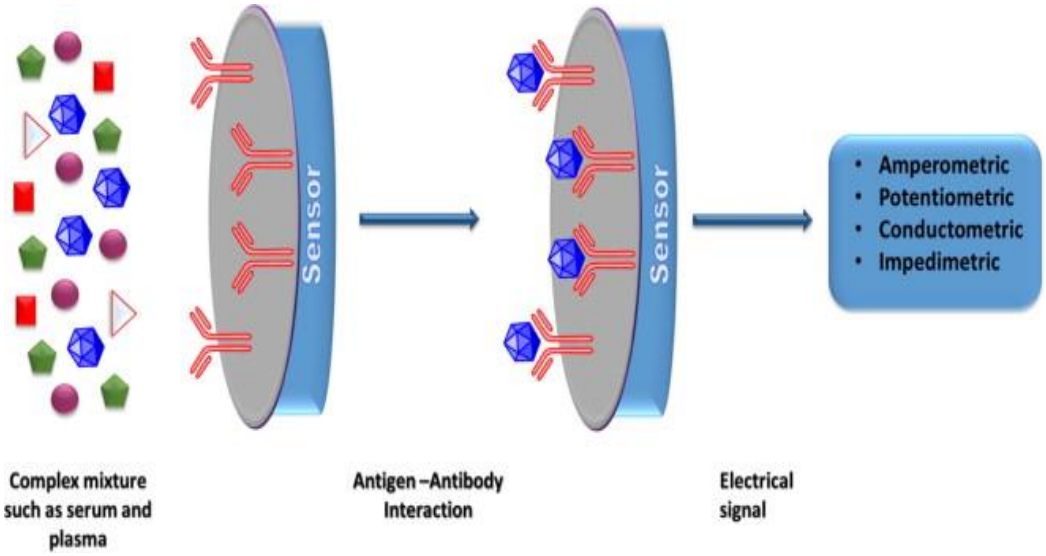

Figure 1.6 Electrochemical immunosensor

Additionally, research has demonstrated that conductive polymers have the ability to significantly increase the conductivity and electron transport rate for 2-Dimensional sheet materials. A lot of research has been done on polyaniline (PANI) because of its

excellent environmental stability and straightforward production. Additionally, polyaniline has a good electrochemical activity, a good large particular surface site, and outstanding Ecofriendly (it contains NH_2, which may bind several antibodies).

Polyaniline (PANI) can be integrated into the intermediate layer of the material based on the 2-dimensional structural features of Molybdenum Disulfide MoS_2, which not only produces a sufficient amount of PANI-MoS_2 heterogeneous interfaces without significantly decreasing the surface of the particular site but also reduces the amount of PANI that is produced.

In the study, a new electrochemical immunosensor based on rGO/ MoS_2@PANI was built and its capacity to detect CEA was tested. High sensitivity, specificity, and repeatability were discovered to characterize the immunosensor's performance in detecting CEA.

The following are immunosensors' key advantages and significance:

i. The combination of graphene and MoS_2considerably increases the electron transport of the electrode-sensitive contact.

ii. More PANI can be embedded into MoS_2/rGO due to its sizable surface area, and PANI provides an abundant site that can be coupled with antibodies to more precisely attach to proteins.

iii. The response signal is increased and the detection signal is stabilized interaction of the optimal ratio of rGO/ MoS_2 and PANI (which contains a lot of -NH_2).

Chapter 2

Literature Review

2.1 Nanoparticles

Nanoparticles are particles with an approximate size of 1 to 100 nanometers. Because of their size, these particles have a variety of features in the nuclear stage. This change in Nanoparticle characteristics is useful in a variety of areas. **[8]** Nanotechnology is foremost thrilling area for researchers in the past century. Since then, a lot of progress has been achieved in the field of nanotechnology. Nanoparticles include well-known polymeric carbon nanoparticles as well as metal, semiconductor, non-metal ceramic, and metal nanoparticles. Due to their high surface-to-volume ratio, small size and nanoparticles differ from bulk substances in both physical and chemical ways. They have a lot of appeal because of their prospective uses in a variety of fields such as catalysis, electrics, ceramics, optics, and magnetism. **[9]**

2.2 Composite

Composites are solid materials that are created when two or more different constituent materials are combined. (**Figure2.1)** Each has its own distinguishing characteristics. (chemical or physical properties) are mixed to generate a new compound with primary qualities that differ from the attributes of specific components within a full structure. **[10,11]**

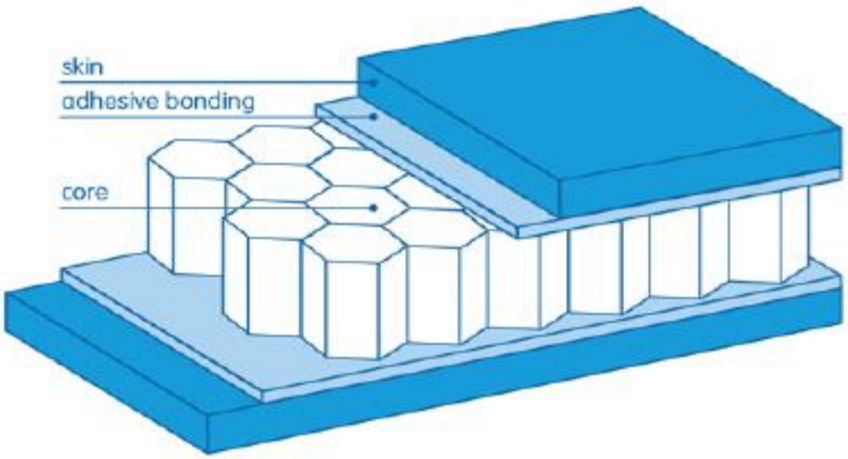

Figure2.1 Sandwich structure of composite **[10,11]**

They are generally designed to provide a wide quantity of traits and properties, a few are as given follows:

i. Growth and Stiffness
ii. Low coefficient of expansion
iii. Resistance in opposition to fatigue
iv. Simple repair to the damaged structure

2.3 Nanocomposite

Nanocomposites are composites that contain a variety of nanoscale morphologic elements such as nanoparticles, nanotubes, or lamellar nanostructures in one stage. They are multiphasic, and multiphasic substances must-have features in the range from 10 to 100 nm on the smallest of scales. In order to overcome the difficulty of having several engine alternatives, nanocomposites can be categorized according to their dispersed matrices and dispersed phase materials. **[12] (Figure2.2)** With the help of these rapidly increasing fields, it is now possible to create a variety of intriguing new substances with unusual qualities using one-of-a-kind new synthetic procedures. The characteristics of the so-called observed objects depend less on those of their object than they did on their morphological and interfacial features. We can't neglect the truth that in some cases, the newly produced characteristic inside the material can be changed without affecting the original constituent substances. **[13,14]** as a result, the idea behind nanocomposite is to use fundamental elements with dimensions in the nanoscale range to make new modern materials with exquisite ease.

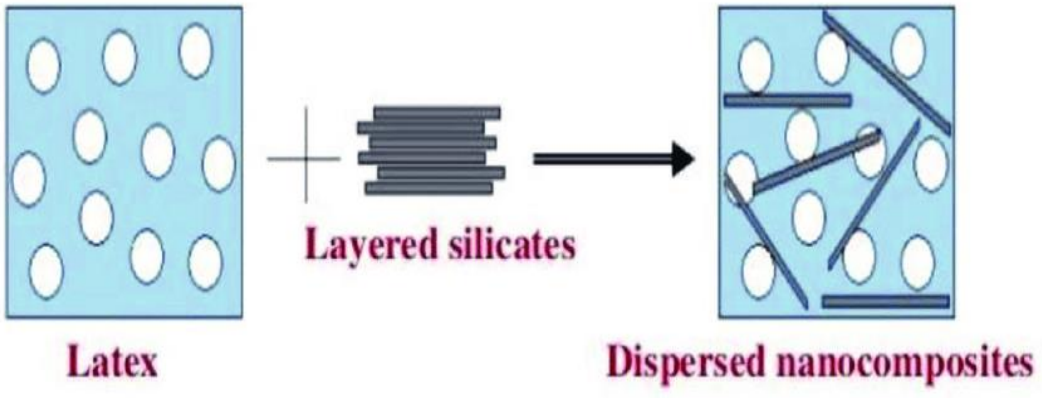

Figure2.2 Formation of Nanocomposite Material **[12]**

2.3.1 Advantages of fabrication novel Nanocomposites

Nanocomposites are made up of a powerful mixture of nanodimensional phase(s) and a bulk matrix with properties that differ due to chemical and structure differences:

- Mechanical and Electrical properties
- Thermal stability
- Reduce smoke generations
- High surface area
- Enhanced electrical conductivity
- Increased chemical resistance

Among many types of nanocomposites, polymeric-based nanoparticles are the most popular in current analysis and events. Polymer-based nanoparticles have an advantage due to traits like film-forming capacity, active functionalities, and dimensional plasticity. **[15]**

The majority of nanocomposites' potential threats occur in areas such as:

- Health and environmental risks
- Production of molecular and structural elements
- Synthesis of polymer-based nanostructured materials

Nanocomposite are the substances that are obtained through the mixture of two or more than two partitioned build in single material provide interesting properties that plausibly emerge from huge surface area, small size and of course from the interfacial interplay of composite between the levels. Their increased potential has been used to boost the biological potential of a variety of medicines, catalysts, biomaterials, and a few high-value contained materials. **[16]**

2.3.2 Types of Nanocomposites

The following labels can be applied to nanocomposite materials, which are essentially dependent on the presence or absence of polymeric material inside the composite.

Non–polymer nanocomposites are those whose compositions don't include any polymer or compounds generated from polymer. **(Fig 2.3)** Non-polymer nanocomposites are the building blocks of non-inorganic nanocomposites. The three categories are metal-based nanocomposite, ceramic-based nanoparticles, and ceramic-based nanocomposite. **[17]**

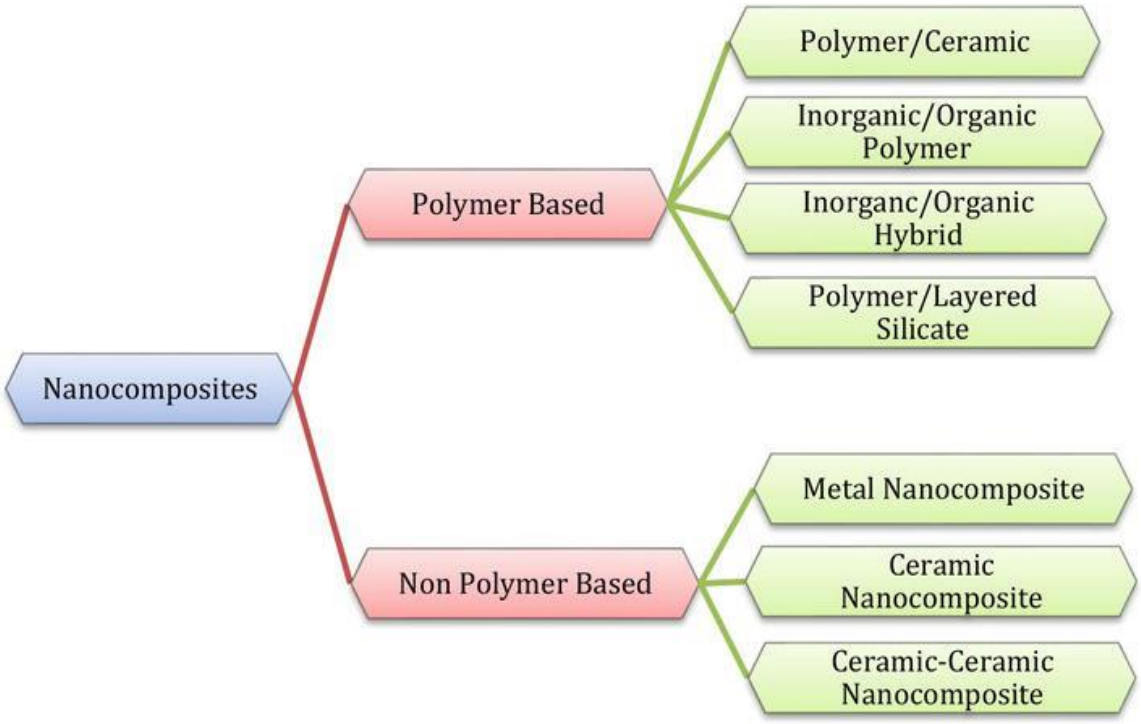

Figure2.3 Classification of Polymer and Non-polymer-based nanocomposite **[17]**

2.4 Non-Polymer-based nanocomposite

2.4.1 Metal-based nanocomposites

Due to its better catalytic features and advantages in optical properties when compared to single and separate metals, bimetallic nanoparticles are widely explored within the framework of either metal alloys or core-shell structures. **[18]**

They can be identified by the following characteristic:

- Superplasticityty
- Low melting point
- Improved in hardness and strength
- Development in magnetic properties

- Increased in electrical conductivity.

2.5 Reduce Graphene Oxide (rGO)

The Nobel Prize in Material Science was awarded to A. Geim and K. Novoselov in 2010 for their discovery of graphene **[19].** Graphene is a possible name for a sheet of carbon atoms made up of condensed sir-membered rings. **(Figure 2.4)** Carbon molecules are sp^2 connected in graphene, forming a hexagonal two-dimensional (2D) lattice **[20].** Single-layer graphene exhibits a unique combination of mechanical, thermal, electrical and optical properties, according to measurements **[21].** Simultaneously, it is crucial for practical applications that can produce significant of high-quality graphene-based materials. To present, only a few graphene synthesis methods have been proposed **[22].** Graphene oxide reduction is one of the most promising approaches (GO Graphene Oxide (GO) is easily accessible and plentiful. It can be made via the Hummers process **[23],** which produces dispersed graphite oxide (GrO) from deep oxidation of natural graphite (Gr). Since the GrO compound's composition depends on its synthesis condition and the nature of the parent graphite, there is currently no significant GrO formula. Its acid-base characteristic and hydrophilicity can be distinguished using the formula $8O_2(H)_2$ when oxygen is present in ketone, carboxyl, epoxy, and other O-containing groups. By ulta power sonication in polar solvents, GrO can easily be exfoliated to GO. A solid reductant, such as hydrazine or $NaBH_4$, is used to reduce graphene oxide to get graphene. Thermochemically reducing graphene oxide (GO) yields reduced graphene oxide (rGO). Every technique has its own set of downsides, such as the use of hazardous compounds, the length of time required, the number of stages required, the high temperatures involved, and the harshness of the environment. We proposed a nontoxic, fast method for removing GO with alcohols in mild circumstances at somewhat low temperatures and pressures.

In this literature, the term "graphene" is used to refer to RGO produced in ways other than the one that was initially suggested. The electroconductivity of (GO) has significantly decreased, and reduced (rGO) that has a high conductivity, which is very useful in immunosensors **[24].** Conglomeration between graphene sheets, on the other hand, is driven by solid stacking interactions, resulting in a tiny specific surface area

and lack of solidity, limiting its assist improvement and widespread application **[25].** In this work of Wei Cao et al., (MWCNTs) are utilized spacers to take into account re-stacking between graphene sheets. The rGO/MWCNTs composites in the study feature a high surface area, robust electron conductivity, and a quick diffusion route for electrolyte molecules **[26].** The introduction of MWCNTs has the potential to provide more active sites for nanoparticles and improve their interaction with the graphene substrate. **[27]**

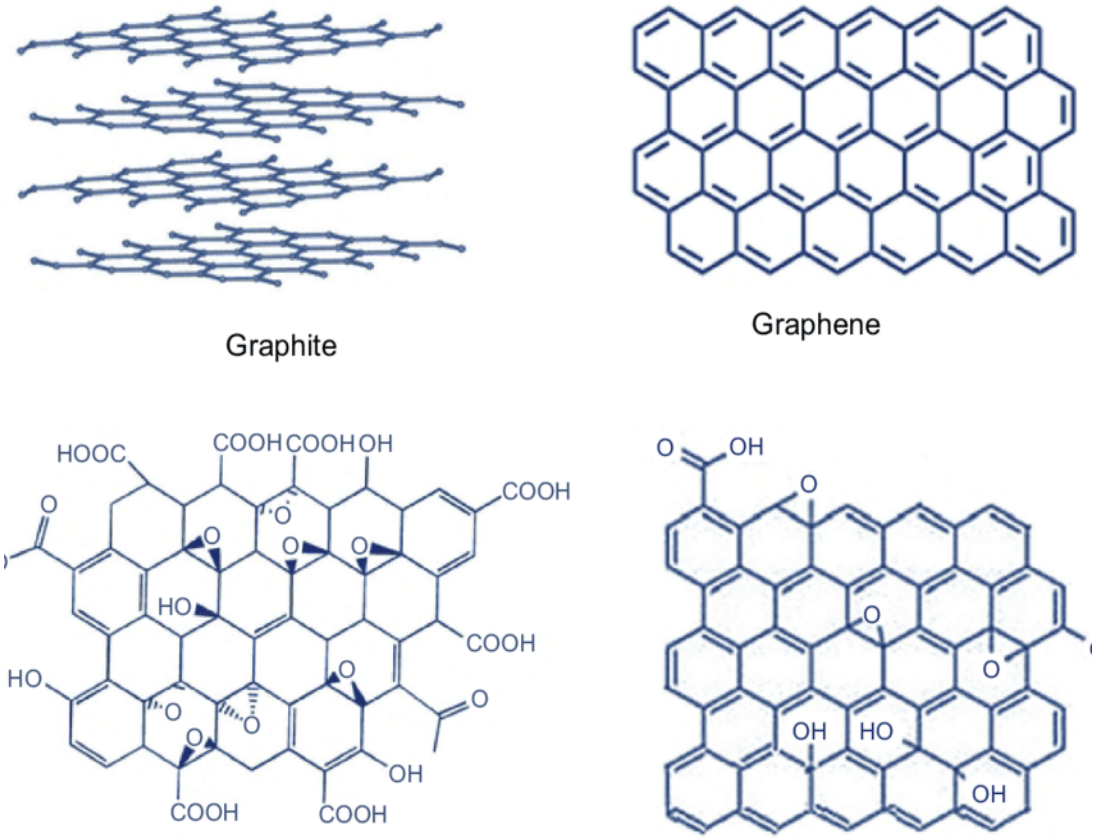

Figure 2.4 Crystal structure of Graphene and Reduce Graphene Oxide(rGO)

2.5.1 Synthesis of Reduce Graphene Oxide (rGO)

A modified version of Hummer's process was used to create GO from powdered natural graphite. First at all, a round bottom flask with an ice bath was filled with 1g of graphite powdered and 1g of sodium nitrate. This time, 26ml of Sulphuric acid(H_2SO_4) was progressively added to the flask using a glass rod. At this point, 16g of potassium permanganate ($KMnO_4$, 99%) was gradually added while being stirred

in a round bottom flask. The flask was placed in a 40^{o}C atmosphere and continuously swirled for 5 hours. The atmosphere was then heated to 95^{o}C and stirred for one hour. Then 60ml of deionized water was added to the flask with a circular bottom. Then 5ml of H_2O_2 was added to the mixture. The round bottom flask was then filled with 20ml of diluted hydrochloric acid (5ml HCL and 15ml deionized water). After that, the solution was centrifuged for 5 minutes at 10,000rpm. After that, deionized water and alcohol were used to wash the sediment until it was litmus-free. Finally, the slid precipitation was placed in a vacuum drying oven for 12 hours at 60^{o}C where it continued to transform into graphene oxide powder.

2.5.1 Applications of Reduce Graphene oxide

- **i.** Wastewater treatment
- **ii.** Corrosion barrier
- **iii.** Energetic materials
- **iv.** Hydrogen storage
- **v.** Biomedical
- **vi.** Batteries

2.6 Molybdenum Disulphide (MoS_2)

TMDs are stacks of sulfur-transition metal-sulfur sheets with a van der Waals strength of 6.5^{o}A that resemble graphene. **(Figure2.5) [28]** Two significant variations of the MoS_2 crystal structure exist: an octahedral structure known as 2H-MoS_2 and a triangular prism crystal structure known as 1T-MoS_2**(Figure 2.6 a, b) [29]** As a result, single strands can be removed from the composites form a shaped into a single-layer morphology. TMDs include molybdenum disulfide (MoS_2). It is made up of a stack of hexagonal Mo particles sandwiched between two layers of S particles and exhibits p-type semiconducting characteristics with poor electrical conductivity. In electrochemical (bio)sensors, MoS_2 has two fundamental benefits. To begin with, it provides more electrochemically dynamic active sites. Second, it can enhance transducer qualities by adding extra components like metal nanoparticles or bio recognition. **[30]** Comparable to graphene material, MoS_2 has diverse affinities towards dsDNA and ssDNA **[31]** Such feature allows MoS_2 to be combined with

widely used aptamer technology. In any event, there are a few disadvantages to 2D MoS_2. Due to their high surface energy, rearranging 2D materials can lead to a decrease in the total number of electrochemically active sites. and their employment as transduction enhancers is constrained by their lack of electrical conductivity. In order to get over the aforementioned issues and create materials with superior electroanalytical capabilities, 2D MoS_2 can be combined with highly conductive materials like graphene. Molybdenum disulfide (MoS_2) has raised extraordinary concern within the areas of electrochemistry since of its excellent electrochemical performance, particularly in the fields of catalysts **[32],** sensors **[33],** electrode materials for capacitors **[34],** and lithium-ion batteries **[35,36].** Taking advantage of their high surface regions, amazing electrical properties, relatively low toxicity, extra active edges, and simple surface modification, MoS_2 being utilized as a perfect matric for developing electrochemical sensor have made an extraordinary achievement.

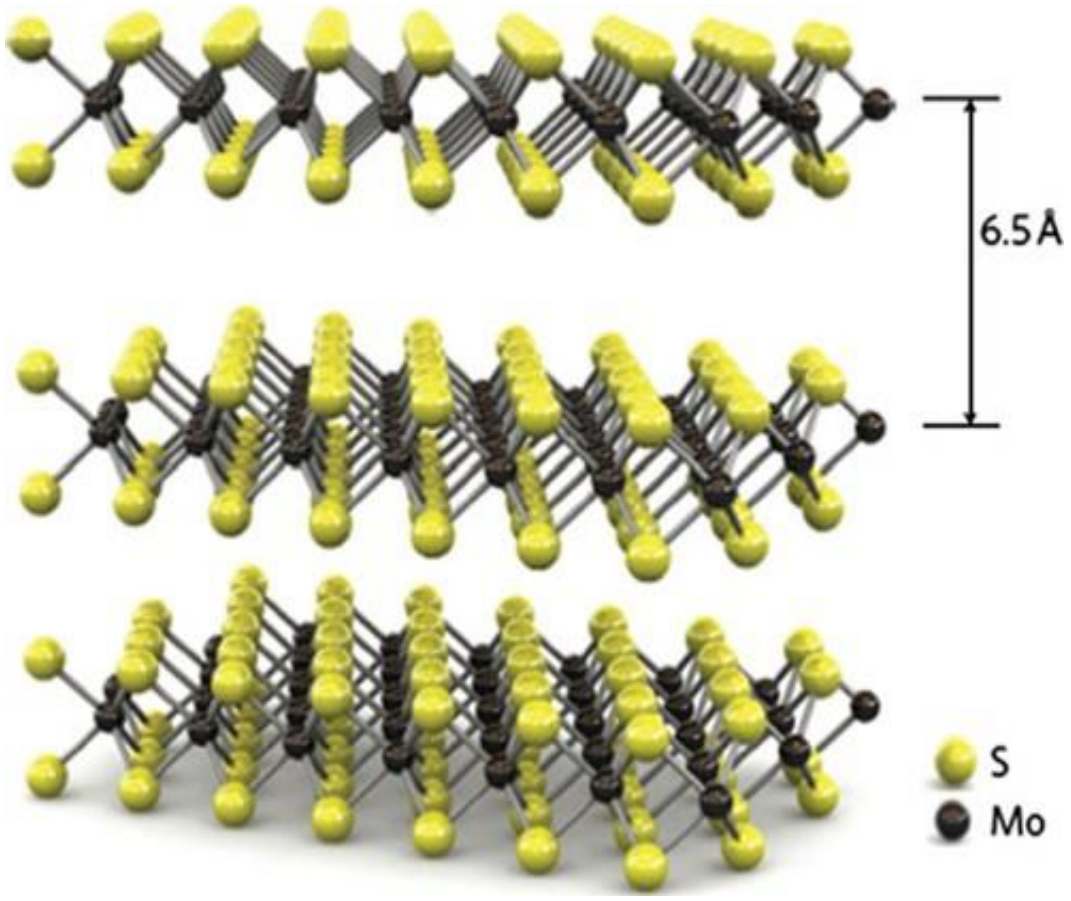

Figure2.5 Illustration of multilayered MoS_2 with an interlayer spacing of 6.5^{o}A **[37]**

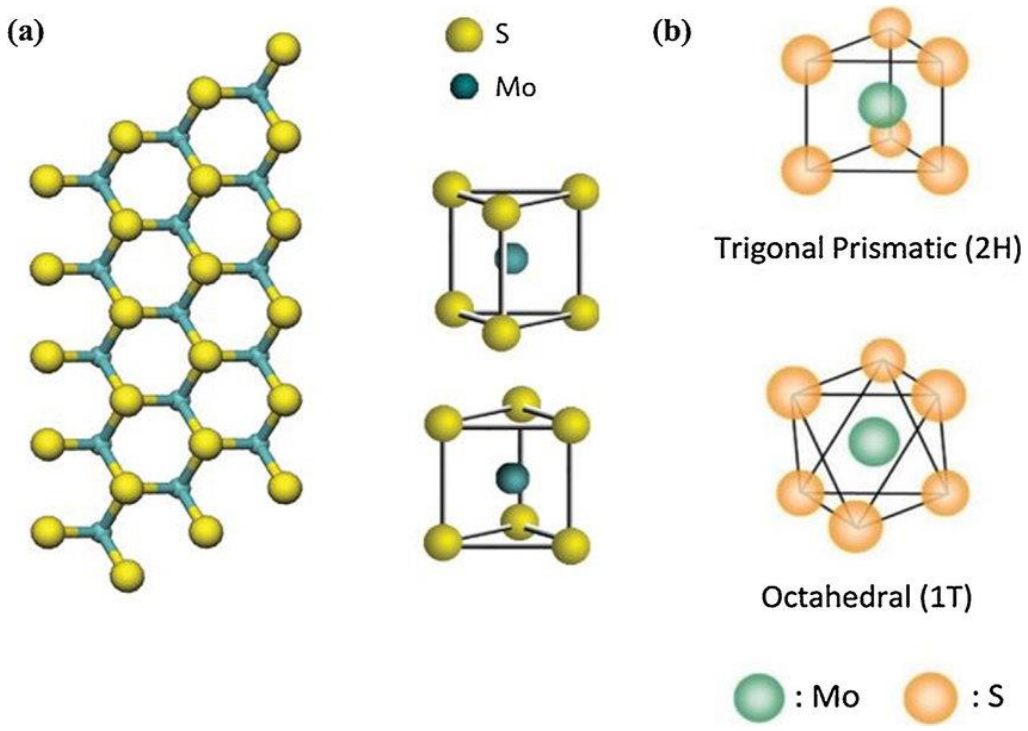

Figure2.6(a,b) Crystal structures of MoS_2 in 2H phase and 1T phase. **[38]**

2.6.1 Synthesis of Molybdenum Disulphide (MoS_2)

The dispersion solution A was created by mixing 319mg of thiourea powder and 185mg of molybdic acid in 30ml of deionized water at room temperature. Put solution A in a 60ml Teflon stainless steel autoclave, tighten the lid, and then heat at 200^{o}C for 24 hours. The particles were thoroughly cleaned three times with deionized water and ethanol before being vacuum-dried at 60^{o}C overnight to produce nanosized MoS_2.

2.6.2 Applications of Molybdenum Disulphide (MoS_2)

i. Solid lubricating **[39]**

ii. Lubricating fluid additives **[40]**

iii. Self-lubricatingating coating **[41]**

2.7 Synthesis of Nanocomposite of MoS_2/rGO

Due to their synergistic effects, MoS_2 and graphene can considerably increase its electrical conductivity **[42].** Ionic liquids (IL) are well-known as eco-friendly reagents with great solubility and high ionic conductivity. The expansion of IL can provide a shielding effect to the-stacking contact between graphene sheets, preventing graphene aggregation and enhancing the interlamellar of graphene and MoS_2, giving

the MoS_2/rGO nanocomposite significantly improved dispersion and electrochemical performance. **[43]**

Table 2.1

LITERATURE REVIEW

Material	**Electrolyte**	**Potential range**	**Scan rate**	**Current density**	**ref**
GO/MoS_2/ Au NPs	0.1M Na_2SO_4	− 0.4 to 0.6 V (vs Ag/AgCl)	10mV/s	3.54 mA/cm^2 (at 0.6V vs Ag/AgCl)	**44**
rGO/ Fe_2O_3/MoS_2	0.5 M H_2SO_4			200 μA/cm^2 (at 0.3V vs Hg/Hg2Cl2)	**45**
PEI–rGO–MoS_2		−0.6 V vs. Ag/AgCl	50mV/s		**46**
MoS_2-PANI/ rGO	0.1M PBS (pH scale 7.0 containing of 0.1 M KCl)	0.2 to 0…8 V	50 mV/s	Anodic peaks at 0.052, 0.196, and 0.304mV. Limit of detection 0.36 mM for UA,	**47**
MoS_2/ rGO /SPE	PBS (pH 7)	168 and 320 mV vs. Ag/AgCl		(4.11, 0.12, and 1.59 μA μM^{-1} cm^{-2})	**48**
TNA/ AuNPs/ MoS_2/ rGO	0.1 M KCl.			0.16 nM limit of detection	**49**

Chapter 3

Experimental

3.1 Objectives

The fundamental goal of this research is to develop electrical sensors that detect uric acid continuously, especially over a wide extent of concentrations, while having a low detection limit and high level sensitivity. The specific goals of the thesis are as follows:

i. Synthesis of a nanocomposite based on Molybedium Disulphide and Reduce graphene oxide.
ii. Characterization of the prepared nanocomposite through different related techniques.
iii. To create a simple electrochemical Uric Acid sensor based on a copper-based Screen Printed electrode and examine the sensitivity of Uric Acid determination.
iv. Investigation of the Cyclic voltammetric response of the modified electrode.

3.2 Hydrothermal Synthesis:

Hydrothermal synthesis is a wet chemical synthesis method in aqueous media to synthesize anhydrous, crystalline ceramic powders. In this process, solution or suspension of precursors in an aqueous medium are treated at elevated temperatures and pressurized containers called vessels. The high temperatures generally range from the water boiling point to the critical temperature of 370°C. At the same time, the pressure can go up to 15 MPa. **[50]** A solution phase is contained by the specific conditions of high temperature and pressure. This results in the rapid phase transformation kinetics in the medium encouraged by mass transport.

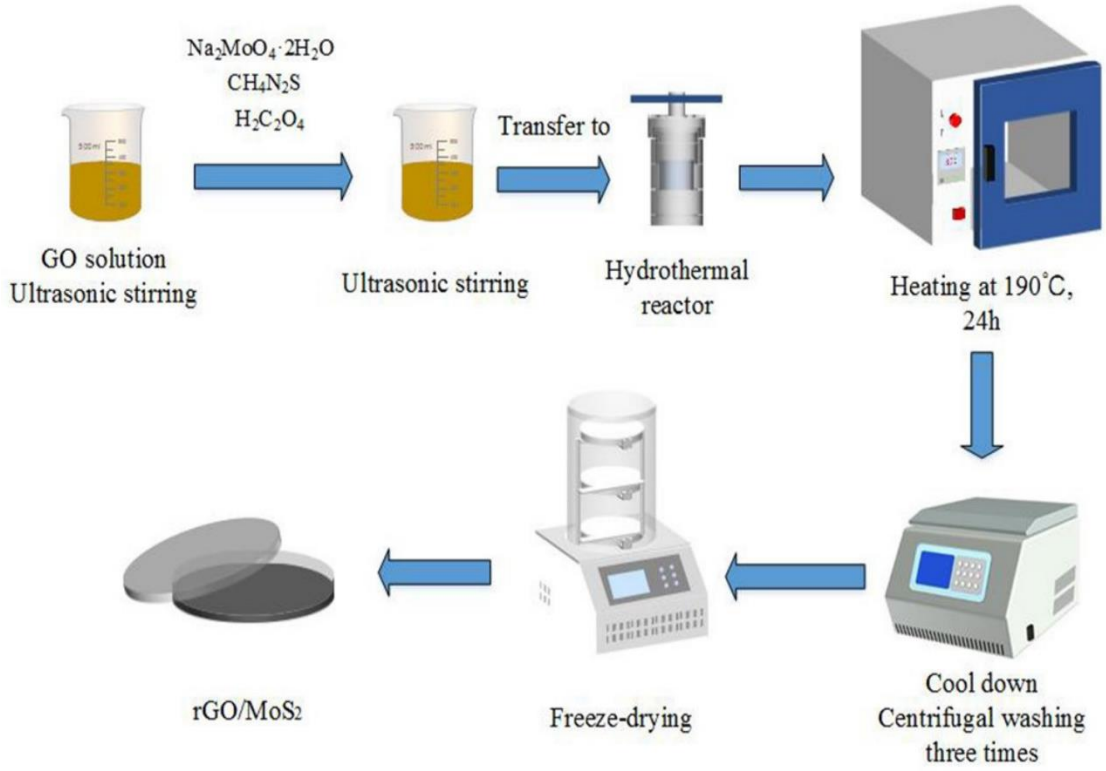

Figure 3.1 Schematic diagram of Hydrothermal reaction

Advantages:

i. More control over the reaction kinetics because of temperature and pressure.

ii. The resulting products have good purity, composition, and morphology.

Disadvantages:

i. Relatively expensive to maintain high temperature and pressure conditions.

ii. High accidental and safety issues because of the operating conditions.

3.3 Chemical vapor deposition

Regular structure is a crucial assurance for the gas sensing capabilities of MoS_2/rGO materials, and chemical vapor deposition (CVD) is an efficient way to create two-dimensional composites with regular structure. By using CVD, it is possible to create MoS_2 and reduced graphene oxide with a two-dimensional lamellar structure. By

altering the reaction conditions, the necessary structure can be produced, and the composite's qualities can be enhanced.

Composite materials can be grown by CVD in two different ways. The first technique involves two steps: first, a precursor based on Mo is placed on a graphene substrate, and then it is sulfurized to produce materials called MoS_2/rGO; the second technique just requires one step. Transition metal Mo and S are gasified to produce MoS_2/rGO materials, which are then produced on a graphene substrate. Thermal annealing was used to create MoS_2 films in a sulphur environment. Mo films' size and thickness can be used to influence the size and thickness of MoS_2 films. It is challenging to find single-layer sheet materials because the MoS_2 films made using this approach are typically multi-layer. Instead of using Mo as a raw material, Li et al. **[51]** used MoO_3, and they thought that MoO_3 was reduced to form MoO_3-x intermediate.

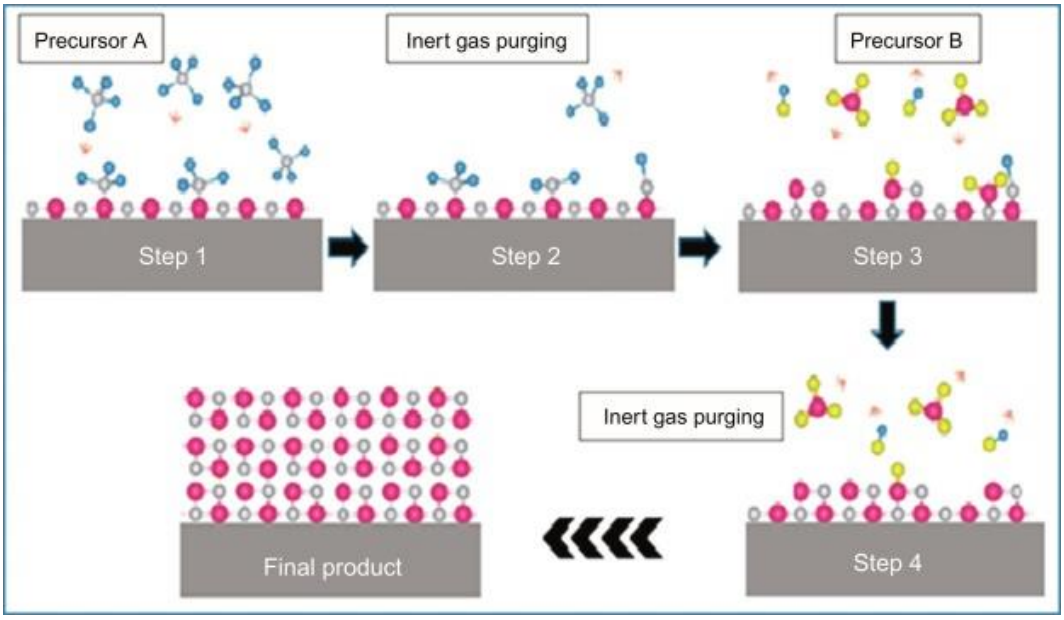

Figure3.2 Schematic diagram of CVD

3.4 Co-precipitation

Co-precipitation the widely used ceramic powder synthesis technique for the preparation of mixed oxides from solution. It starts by forming a supersaturated solution that containing the precipitating agent. The resultant precipitated powder is filtered from the solution followed by drying. Then thermal decomposition of the powder to get the required ceramic. The co-precipitation reaction can be controlled by

several parameters, such as temperature, pH level, concentration, and mixing rates of the precursors. **[52]**

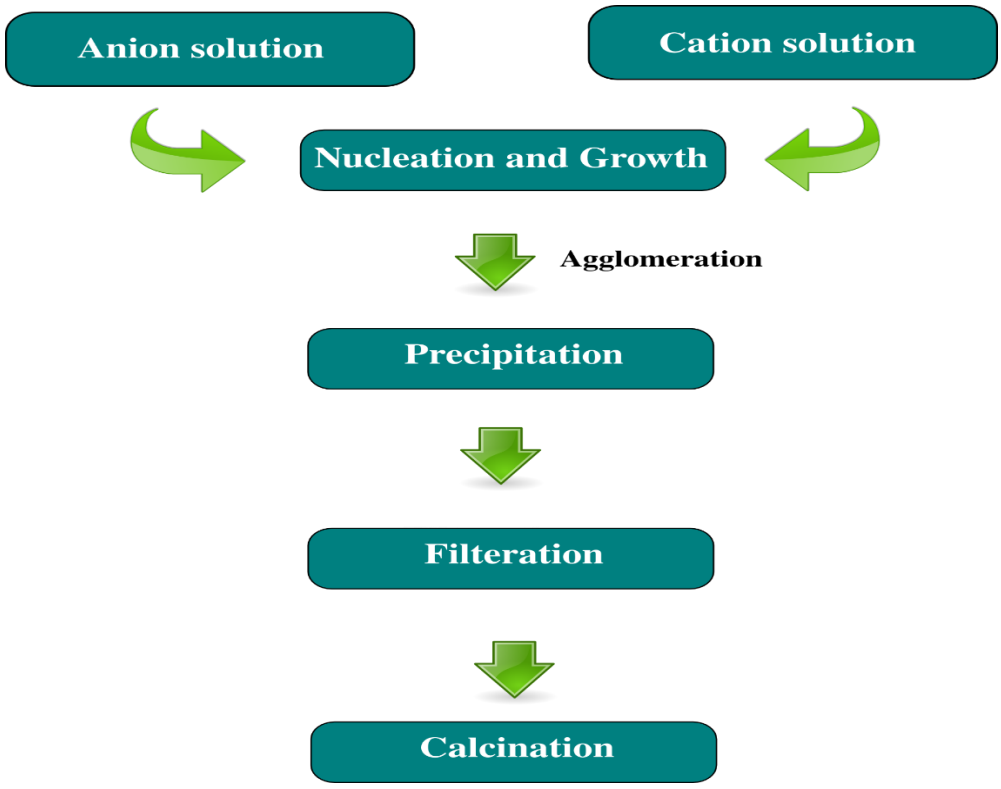

Figure 3.3 Flow chart of Co-precipitation method

Advantages:

i. The resulting products have good purity, composition, and morphology.

ii. By controlling the reaction parameters, fine particle size with good purity and narrow size distribution can be produced.

iii. Relatively inexpensive to produce a high-quality produce.

Disadvantages:

i. Microscopic inhomogeneity can be caused due to the difference in the rate of precipitation of individual compounds.

ii. Calcination can generally result in agglomerates, which is in common with other synthesis techniques.

3.5 Drop Casting method

Using the drop-casting method, RGO materials were effectively self-assembled by evaporating the solution to produce flexible and conductive films. When a MoS2/rGO molecule was first applied to the substrate, MoS2/rGO sheets initially naturally self-assembled at the interface region, producing a MoS2/rGO film as the water evaporated from the aqueous dispersion. As a result, the MoS2/rGO film may be used to cover the modified SPE. When an aqueous solution droplet is sprayed to a solid surface, it progressively dries into a dense, ring-like deposition along the circumference, creating the "coffee-ring" appearance. However, the drop-casting technique rarely manages to control the homogeneous of the MoS2/rGO layer on the substrate. In the study, it was shown that the RGO film's interaction with the altered substrates was beneficial for reducing the unequal buildup of MoS2/rGO sheets. The four different types of SPE substrates that were looked at were unmodified SPE, SPE covered with MoS_2/rGO, SPE modified with a carboxyl group, and SPE modified with an alkyl group. The ultrathin adhering MoS_2/rGO layer was created by Lee, Dellatore, Miller, **[53]** and Messersmith (2007) by immersing SPE substrates in a uric acid solution. According to Kim, Lee, et al. (2011), the MoS2/rGO layer's catechol group may be crucial for a universal surface attachment onto substrates with low surface tension. These substrates can interact with organic substrates in a variety of ways, including covalent bonding and strong non-covalent interactions like hydrogen bonds (Ye, Zhou, & Liu, 2011). On SPE substrates coated with MoS_2/rGO, this might make it possible to make flexible, transparent, and sheet-resistant MoS_2/rGO films with ease. The same method can be used to make RGO films on various modified SPE substrates.

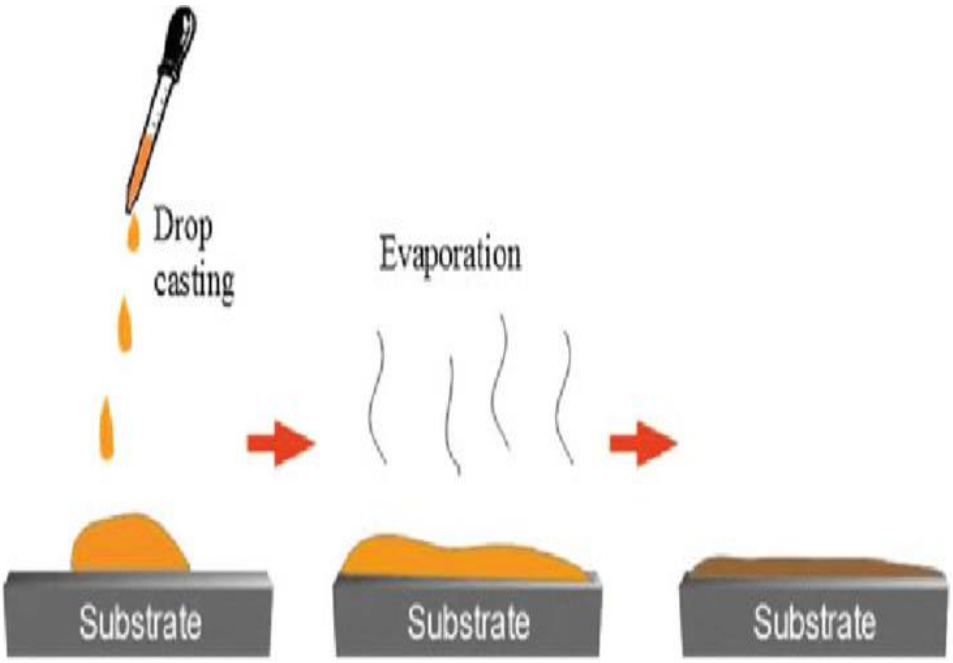

Figure 3.4 Schematic diagram of Drop casting method

3.6 Sol-gel:

This process involves preparing amorphous gel made from the solution, which is then dehydrated at low temperatures. Precursors like metal oxides and salts are hydrolyzed in a gelation agent leading to cross-linking and branching. A dense three-dimensional structure results from the polymerization reaction, which preserves the mixing and results in controlled composition at molecular state, avoiding any segregation. Composition is maintained at the molecular level through the gelation process because of the soluble nature of initial precursors. **[54]** Then the gel containing a three-dimensional matrix is dried by heating at low temperature. The temperature is usually lower than in any other synthesis technique.

Figure 3.5 Schematic diagram of Sol-gel

3.7 Chemicals and Materials

Reduced graphene oxide was procured from Sigma Aldrich, molybdenum Disulphide MoS_2 was procured from Sigma Aldrich, $Na_2MoO_4.2H_2O$ (Molybdic acid sodium salt dehydrate) was procured from Sigma Aldrich, NH_2CSNH_2(Thiourea) were procured from Sigma Aldrich, double distilled water. N, N-dimethyl formamide (DMF) (5%) and HCl respectively, Uric acid(2,6,8-Trihydroxypurine) was purchased from Avonchem (98%), ultrasonicator machine, Micro peppite, Screen printed copper-based electrode coating, Deionized water, stirrer machine. The materials were used as-received with no further processing.

3.8 Synthesis of MoS_2/rGO Nanocomposite

The chemical production of a hybrid novel nanocomposite made up of molybdenum Disulphide and reduced graphene oxide (MoS_2/rGO) is described. Briefly, in a beaker containing 100ml of Distilled water, 50mg powder of rGO nanoparticles were dispersed in the beaker and ultrasonicated the solution until the mixture would become yellow-brown and showed rGO aqueous suspension was obtained. After a little time, 0.6 g of $Na_2MoO_4.2H_2O$ (Molybdic acid sodium salt dihydrate) and 0.75 g of NH_2CSNH_2 (Thiourea) were dissolved in the aforementioned rGO suspensions solution (30 mL) and agitated until a homogenous solution was obtained. After that,

the MoS_2/rGO solution was transferred to a 100mL Teflon autoclave and cooked in an oven for 24 hours at 180°C. The black precipitates were obtained after becoming less heated at room temperature naturally, centrifuged, washed with distilled water, and then dried under a vacuum at 50°C overnight.

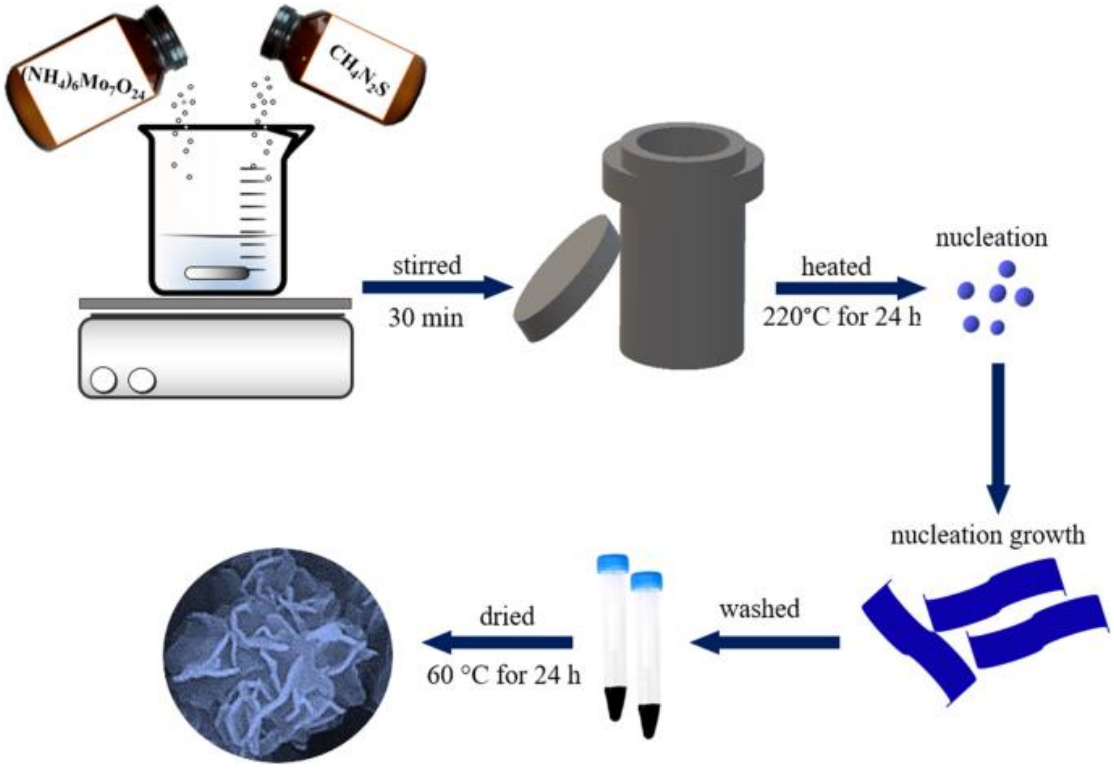

Figure 3.6 Schematic diagram of MoS_2/rGO synthesis

3.9 Preparation of Modified Electrode

Earlier in the estimation, we prepare the mixed solution of DMF/H_2O (the volume ratio of water vs DMF was 1:3) to enhance the adhesive properties or surface coating. The dried MoS_2/rGO nanocomposite was dispersed in a DMF/H_2O mixed solution after some time, and then ultrasonically homogeneous in the mixed solution. The concentration of nanocomposite suspension was 10mgmL^{-1}. At that point, 10µL of suspension is cast onto an SPE (copper-based) and dried under natural light at room temperature.

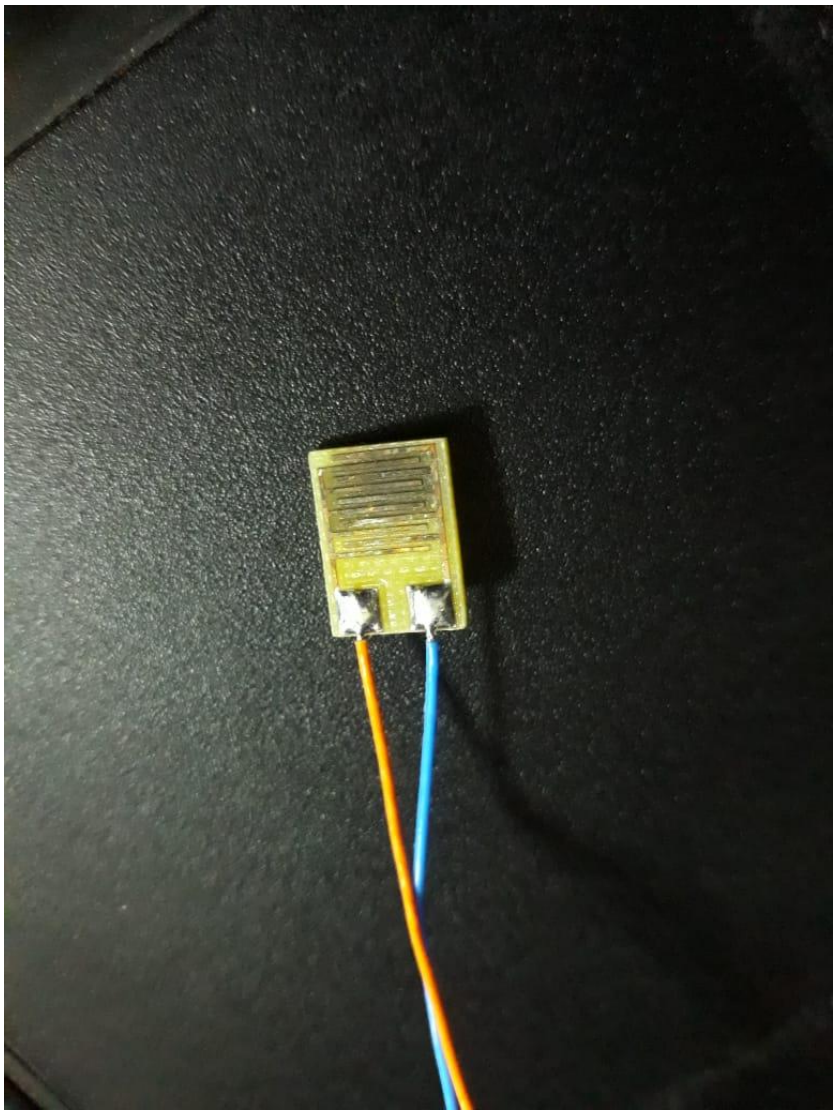

Figure 3.7 Schematic diagram of MoS_2/rGO@Screen printed electrode

Chapter 4

Characterization Techniques

4.1 Instrumentation and measurement

The tests of morphological studies were assessed using SEM on a JEOL JSM-6490A. (Tokyo, Japan). A Seimens D5005 STOE &Cie GmbH (Darmstadt, Germany) was used to analyse the molecular structure data using X-ray diffraction (XRD) at an angle (2θ) between 10^{o} to 80^{o}. Using dry powder testing and potassium bromide pellets, the FTIR analysis was performed using a PerkinElmer Spectrum TM 100 spectrophotometer. A typical electrode configuration with a modified SPE as the working electrode, copper wire as a counter terminal, and a reference terminal was used in the electrochemical behavior of the prepared experiments. (Interface 1010E potentiostat, USA).

4.2 Scanning electron microscopy (SEM)

4.2.1 Overview

The foremost broadly utilized technique for the characterization of different materials is scanning electron microscope (SEM) which utilizes a raster scan pattern to scan the surface of a test with a high-energy electron beam to create a high-resolution image. The image produced by the electrons interacting with the surface of the sample test under examination reveals data with respect to the sample such as the surface topography and chemical composition.

4.2.2 Working principal

To make the SEM images, electrons are generated within the electron gun, as a rule, a V-shaped thin tungsten filament served as a source of electrons, a so-called thermionic cathode that is heated up by the electric current to gain the emissions of electrons. The generated electrons are centered on an anode. Between the anode and

the thermionic cathode, a voltage distinction is connected in which the anode is connected to a positive pole and the cathode to a negative pole of a high voltage source. This voltage distinction is known as the accelerating voltage that has a value between 0.2 and 40 keV, finding out the wavelength and energy of electrons inside the beam.

The solid electric field between the cathode and the anode accelerates the electrons (known as incident primary electrons) to hit the test sample which discharges different types of emissions from the surface of the sample: *backscattered electrons* which have kinetic energies about the same as that incident beam between 50eV and *secondary electrons* that have possessed energy less than 50eV, *augur electrons* that are delivered by the de-excitation of particles, and *characteristic X-rays* that are moreover produced by the de-excitation of atoms by releasing the additional energy. The chemical composition of a test sample can find through X-ray energy, which is particular to the element from which it was discharged.

Secondary electrons are profitable in SEM imaging because it is responsible for appearing the topography and morphology of the test. The incident primary electrons after striking the surface of a test sample causes the electrons from the surface to remove. These removing electrons are called secondary electrons which are collected by a secondary electron detector (SE detector) joined to a positively biased grid and interpreted into signals which are further amplified, interpreted, and changed into an image (**Figure 4.1**).

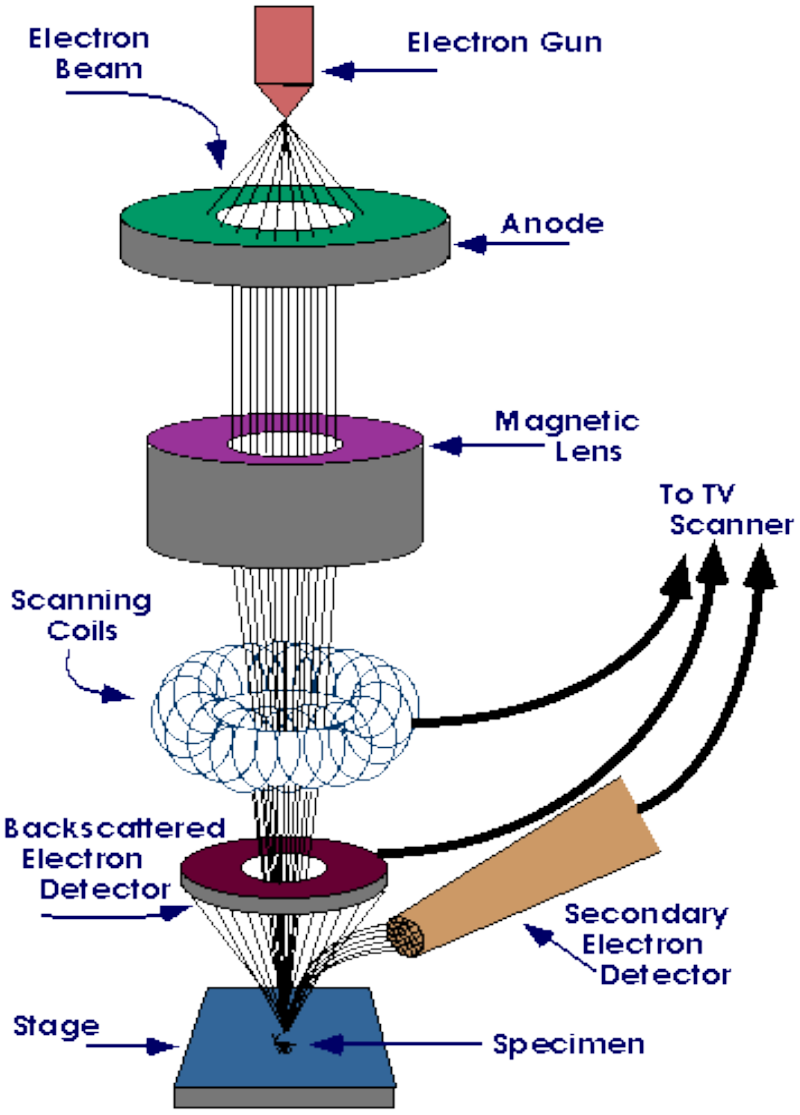

Figure 4.1 Schematic diagram of SEM

4.3 X-Ray Diffraction (XRD)

4.3.1 Overview:

X-ray diffraction may be a powerful non-destructive method used for the characterization of materials utilizing x-rays radiations. X-rays are electromagnetic radiations of precisely the comparative nature as light but with high energy and a very shorter wavelength of approximately 1Å. Max Von Laue and his colleagues discovered in 1912 that crystalline substances function as three-dimensional (3D) diffraction grating at X-ray wavelength that are similar to the interplanar spacing inside a crystal lattice.

XRD is utilized for the identification of the present crystalline stages in material and

their basic structural properties. It is also utilized for the accuracy of microstructure investigation of polycrystalline and amorphous materials, unit cell dimensions, average particle size, film thickness, and sample purity.

4.3.2 Working Principal

The test to be analyzed is illuminated with a beam of X-rays (**Figure 4.2**). As parts of materials are made up of little crystals which are made up of the regular arrangement of particles and each atom is comprised of nucleus clouds of electrons. When the x-rays experience an atom, the electrons oscillate by the impact of the incoming x-rays and ended up as secondary sources of x-rays with the same energy as the incident. Depending on whether the waves are aligned or not when X-rays are connected to one another, the signal may be enhanced or destroyed. When the waves are aligned, constructive interference occurs, which amplifies the wave signal; when the waves are not aligned, destructive interference occurs, which destroys the wave signal. The arrangement of atoms in a crystal forms different planes are separation by clear or well-defined. The widely spread atoms weakens the X-rays when they are focused on atomic planes. At exceptionally specific angles where the scattered waves constructively interfere, the radiated signals are intensified significantly. typically known as diffraction. The diffracted x-rays are recorded by recorded within the frame of a graph.

The x-rays diffracted from crystal are depicted by the condition known as Bragg's law:

$$n\lambda = 2d\sin\theta \quad \text{……(4.1)}$$

Where n denotes to the reflection arrangement, λ is the wavelength, d denotes to the crystal lattice planes interplanar distance., which is responsible for a particular reflector wave on the screen, and θ denotes the angle between the lattice planes and incident beam.(**Figure 4.3**).

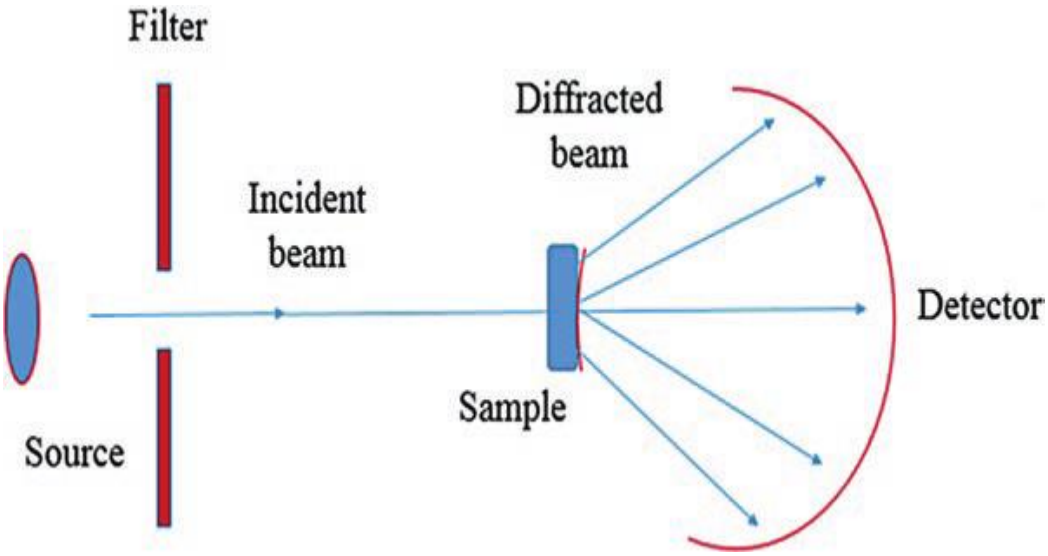

Figure 4.2 Schematic diagram of X-ray diffraction

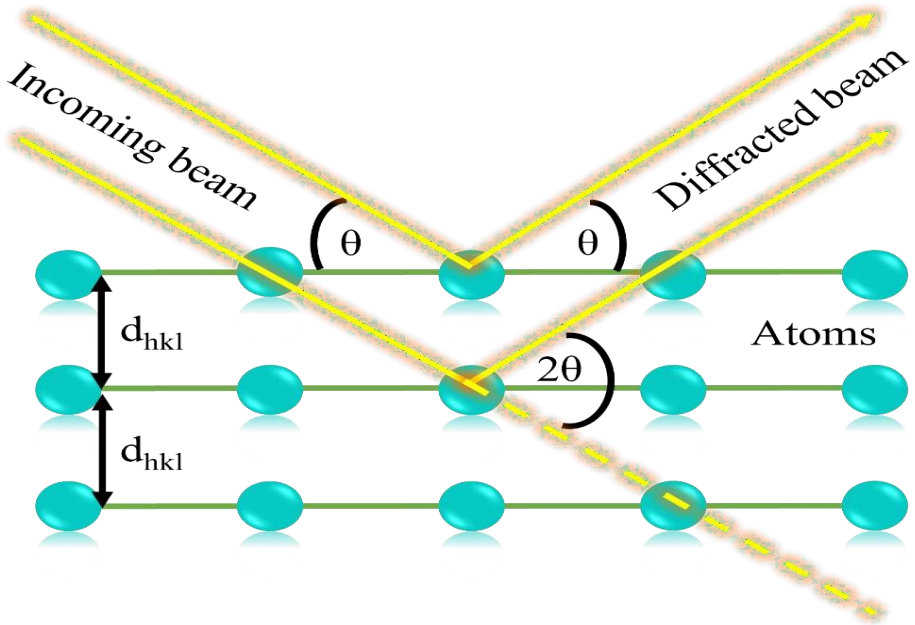

Figure 4.3 Schematic diagram of a Bragg's law **[55]**

The procedure of this experiment includes the crushing of samples into fine powder. Afterward, the model will be placed on an aluminum or glass rectangular-shaped plate. A monochromatic X-ray beam is then directed towards the powder sample.

Lattice Constant:

Crystal unit cell called lattice constant. Angle forming between two edges or the length of one edge. It is also called the lattice parameter. The lattice constant is the

distance between the lattice points; the following equation calculates the lattice constant.

$$\alpha = \frac{\lambda(h2+k2+l2)1/2}{2sin\theta} \ldots\ldots\ldots\ldots\ldots\ldots (4.2)$$

The above equation shows that lattice constant is (**α**) the wavelength of X-ray incident is 1.54Å for Cuk (**α**), miller indices

Crystallite Size:

For the identification and confirmation of the experimentally obtained diffraction pattern, it is compared to JCPDS cards. The structural properties are greatly influenced by particle size. The XRD perfectly measures the homogeneous and inhomogeneous peaks of the nanomaterial. Strains in the inhomogeneous material vary from crystal to crystal within a single crystal and by increasing angle the broad range of diffraction peak. Scherer's formula can be used for the calculation of crystallite size D can be estimated from peak width.

$$D = \frac{K\lambda}{B\ Cos\theta} \ldots\ldots\ldots\ldots\ldots\ldots (4.3)$$

B in the above equation denotes full width half maximum.

θ is the angle called diffraction angle.

K is known as Scherer's constant depend upon crystal size.

X-Ray density:

Using XRD, material density can be found, and by applying the formula, we can calculate the material density if lattice constant α know for each sample.

$$\rho_x = \frac{8M}{Na3} \ldots\ldots\ldots\ldots\ldots\ldots (4.4)$$

Measured Density:

The measured density tells us about the intrinsic properties of materials that define bulk density or measured density. The formula generally used for calculation

$$\rho_m = \frac{m}{\pi r2h} \ldots\ldots\ldots\ldots\ldots\ldots (4.5)$$

'm' represents mass, 'r' represents the radius, 'h' represents the thickness of the pressed pallet.

Porosity Density:

Porosity density shows the pellet's strength and the state or property of being porous. By increasing the concentration of doping material in the sample, the porosity fraction increased. By using the formula

$$\textbf{Porosity fraction} = 1 - \frac{\rho m}{\rho x} \ldots\ldots\ldots\ldots\ldots\ldots (4.6)$$

4.4 Fourier Transform Infra-Red (FTIR) Spectroscopy

4.4.1 Overview

Infrared spectroscopy analysis the interaction between infrared radiation and matter. This Infrared radiation is electromagnetic radiation with a larger wavelength as compared to a shorter wavelength. FTIR is the foremost broadly used as a vibrational spectroscopic technique for distinguishing the functional groups or the sorts of chemical bonds. It is the sort of infrared spectroscopy in which the Fourier transform strategy is utilized to secure an infrared spectrum in an entire range of wavenumbers altogether. It shifts from the dispersive strategy, which includes making a spectrum at a single wavenumber separately by collecting signals. At present, FTIR has nearly completely replaced the dispersive strategy since FTIR contains a higher signal-to-noise proportion than the dispersive technique.

IR radiation is produced by a light source and coordinates at the sample which absorbs the particular amount of passing light while few lights are reflected. The remaining light is transmitted having the molecular data and collected by a detector to create an electronic signal.

4.4.2 Working principal

The Michelson interferometer is an important portion of the Fourier transform infrared spectrometer. The IR beam from the source enters the interferometer and is centered on a beam splitter during the measurement as illustrated in **Figure 4.4**. The beam is split and directed toward a stationary and movable mirror, individually. After

that, the beam is recombined and coordinated with the sample material. The spectral information of all the wavelengths is procured at the same time. The moving mirror changes the optical path of lengths to produce light interference within the two split beams. The optical ways of both split beams are at the same father moving mirror is found at a comparative separate from the beam splitter as the fixed mirror; hence, there's zero path difference. An optical path difference (δ) can be made by shifting the moving mirror distinct from the beam-splitter. The destructive and constructive interference will be produced by the two splitting beams, hence the value of **δ** will be changes consistently.

Constructive interference occurs when;

$$\boldsymbol{\delta = n\lambda,}$$

whereas when;

$$\boldsymbol{\delta = (1 / 2 + n)\ \lambda}$$

at that point, destructive interference occurs. A change within the position of the moving mirror results in a change in the δ esteem.

FTIR spectrometer is operated on the principal know as Fourier transform. Mathematically expressed by.

$$\mathbf{F\ (\omega) = \int_{-\infty}^{+\infty} f(x)\ e^{i\omega x} dx} \ldots\ldots\ldots\ldots\ldots\ldots (4.8)$$

And the conflicting form of this equation is

$$\mathbf{F\ (\omega) = \frac{1}{2\pi} \int_{-\infty}^{+\infty} f(x)\ e^{-i\omega x} dx} \ldots\ldots\ldots\ldots\ldots\ldots (4.9)$$

ω is the regularity.

X is ophthalmic path variance.

F (ω) is the spectrum.

$f(x)$Is the interferogram. **[56]**

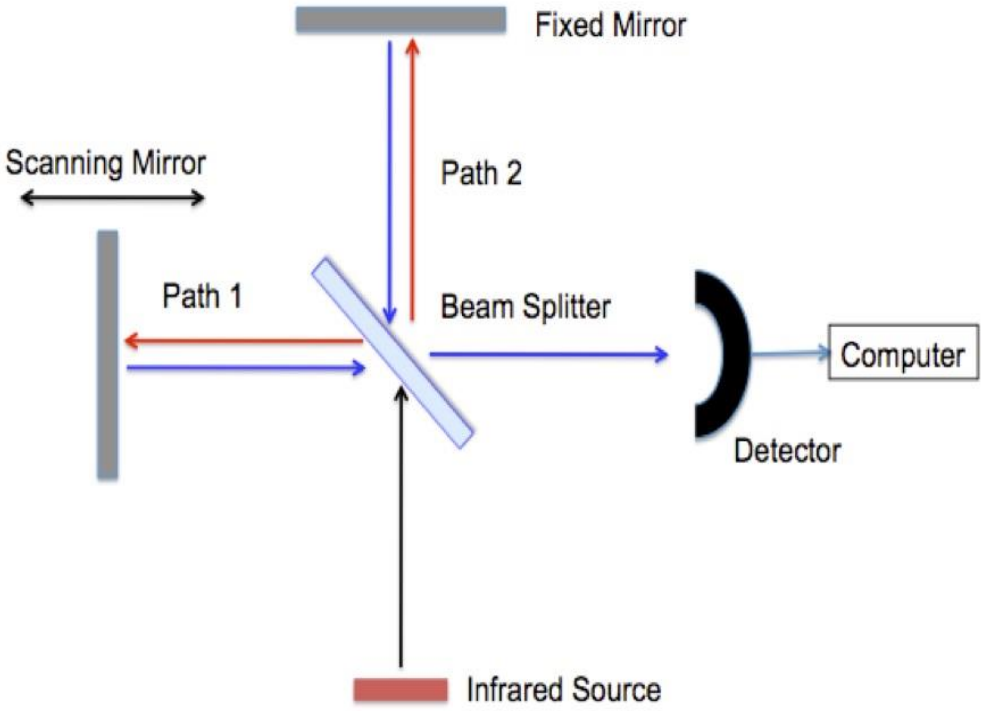

Figure 4.4 Schematic representation of an FTIR

A graph of light interference escalates as a function of optical way contrast is known as an interferogram. The infrared range, which may be the graph of light intensity against wavenumber, must be Fourier transformed from an interferogram. Interferogram signals are gotten by the FTIR detector and sent to a test (or reflected from a test material). The interferogram of the detector doesn't incorporate an infrared spectrum. A computer device with FTIR makes the infrared range using the quick Fourier transform (FFT) calculation. There are three main types of FTIR.

i. Transmission FTIR spectroscopy.

ii. Emission FTIR spectroscopy.

iii. Reflectance FTIR spectroscopy. **[57]**

The detectors are used in FTIR are much more sensitive rather than other optical IR optical devices. Only one mirror is moving in FTIR, so its minimum chances of mechanical breakdown. The measurements made by FTIR are extremely accurate and highly reproducible. It has made possible the development of many new sampling techniques.

The FTIR spectrum can be compared to a chemical fingerprint mark. It can be utilized to distinguish and confirm unknown and known samples, and as well as to characterize unused materials. Particularly valuable within the chemical and fabrication industries, and as well as in research and improvement in development. various analytical questions in an assortment of industries can be replied to utilizing FTIR spectroscopy, supportive on the spectrometer setup and method.

Sample Preparation for FTIR:

KBr pellets method used to prepare samples for FTIR; alkali salt shows zero absorption in IR spectrum. The potassium salt (KBr) was placed in an oven at 100 °C for one hour to remove any absorbed moisture. Sample and KBr were mixed and ground to fine powder at a 1/4 ratio, respectively. Pellets were prepared using a pellet die of 13 mm diameter. The mixed powder was placed in the die and compressed by applying pressure of 1 metric ton for 45 seconds from the hydraulic pump. Finally, a thin sample pallet having a thickness in the range of 2-3 mm and a diameter of 13 mm was obtained.

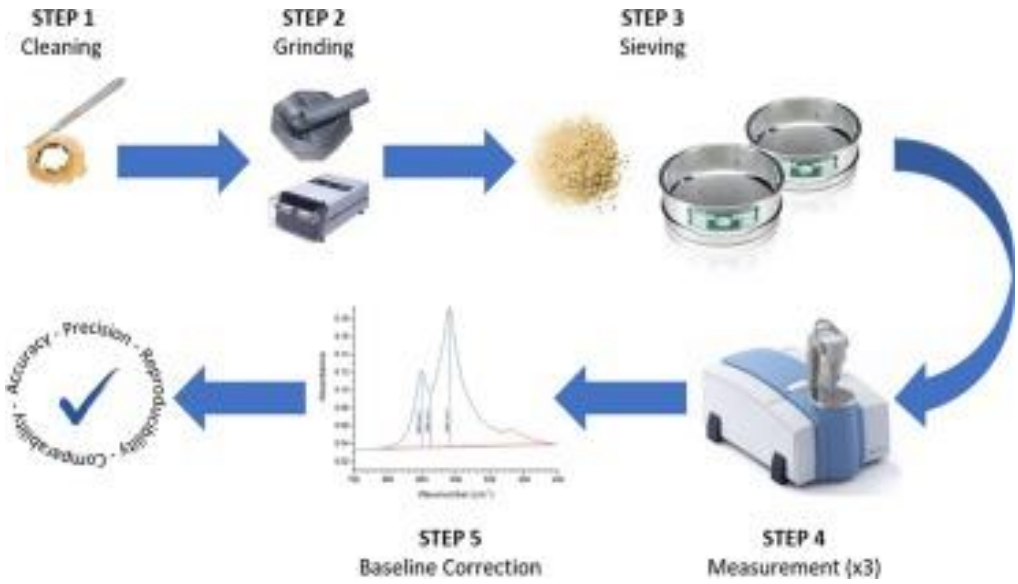

Figure 4.5 Schematic of sample preparation of FTIR.

4.5 Cyclic Voltammetry (CV)

4.5.1 Overview

Cyclic voltammetry (CV), a type of potential sweep strategy, is the foremost

commonly utilized electrochemical method employed to get preliminary information almost the electrochemical process. Different processes such as the redox process of electrode materials as well as reactants and kinetics of heterogeneous electron exchange reaction that happens in an electrochemical cell can be decided through the CV.

4.5.2 Instrumentation

The cyclic voltammetry system consists of:

i. *Electrolysis cell:* An electrolysis cell comprises an electrolytic solution, counter electrode, reference electrode and working electrode. Amid the reduction and oxidation reaction, the electrolytic solution gives ions to the electrodes. The working electrode has a feature of a metallic surface with a well-defined range where the response of interests takes place. The working electrode potential changes linearly with time, whereas the reference electrode potential remains constant. The reference electrode does not take a portion within the reaction and does not draw current. The counter electrode is capable of conducting electrical power from the signal source to the working electrode.

ii. *A potentiostat:* A potentiostat is an electrical instrument that utilizes a direct current (DC) power source to preserve and precisely determine a potential whereas too letting little currents be drawn into the framework without influencing the voltage

iii. *A current-to-voltage converter:* It is utilized to determine the output current.

iv. *Data processing system:* The framework employed to produce the resulting voltammogram.

4.5.3 Working principal

To perform cyclic voltammetry, a reference solution in conjunction with the electrolyte solution and the three electrodes is included in an electrochemical cell. The potential between the reference and working electrode is clearly straight using a potential until it approaches a preset restrain, from which it is clearly back oppositely.

4.5.4 The Randles-Sevcik Equation

The Randles-Savcik equation depicts the reversible redox process, peak current ip at 298K, the Randles-Savcik condition is:

$$i_p = (2.69x10^5)\, n^{3/2} A C D^{1/2} v^{1/2}$$

Here n the number of electrons, A shows the electrode surface area (cm^2), D represents the diffusion coefficient ($cm^2.s^{-1}$), C shows the concentration of ($mol.cm^{-3}$), and v is the potential scan rate ($V.s^{-1}$)

4.5.5 Applications

CV can be utilized to investigate qualitative information regarding electrochemical processes under different conditions, counting reversibility of a reaction and the nearness of intermediates in oxidation-reduction responses. A CV moreover is utilized to determine the diffusion coefficient of analysis, the electron stoichiometry of a framework, and the decreased potential which can be utilized as a device for identification. Additionally, since the concentration in a reversible (Nernatian) framework is proportional to the current, the concentration of an unknown solution can be determined by producing a calibration curve of concentration versus current.

Chapter 5

Results and Discussion

5.1 X-ray diffraction

The crystal structure of MoS_2, rGO and MoS_2/rGO nanocomposite were examined using X-ray diffraction(XRD). The diffraction peaks of the nanocomposite are comparable to those of the standard cards for rGO (JCDPS 05-0566) and MoS_2 (JCDPS 37-1492). Both samples had a comparable conventional hexagonal structure of crystalline MoS_2 and rGO as seen in Fig.5.1. When compared to the diffraction from the rGO and MoS_2 with a layer-to-layer separation of 0.62 nanometer, the major peak of both appeared approximately 27°. It demonstrates that the diffraction peaks at 27°, 32.8°, 39.5°, 50.3°, 56.1°, 58.3°, 60.3°, 69.0°are associated with the MoS_2 crystal faces (002), (100), (103), and (105). The rGO peak at 10.1° may be blocked by the other higher peak, therefore there isn't a clear diffraction peak of the rGO.

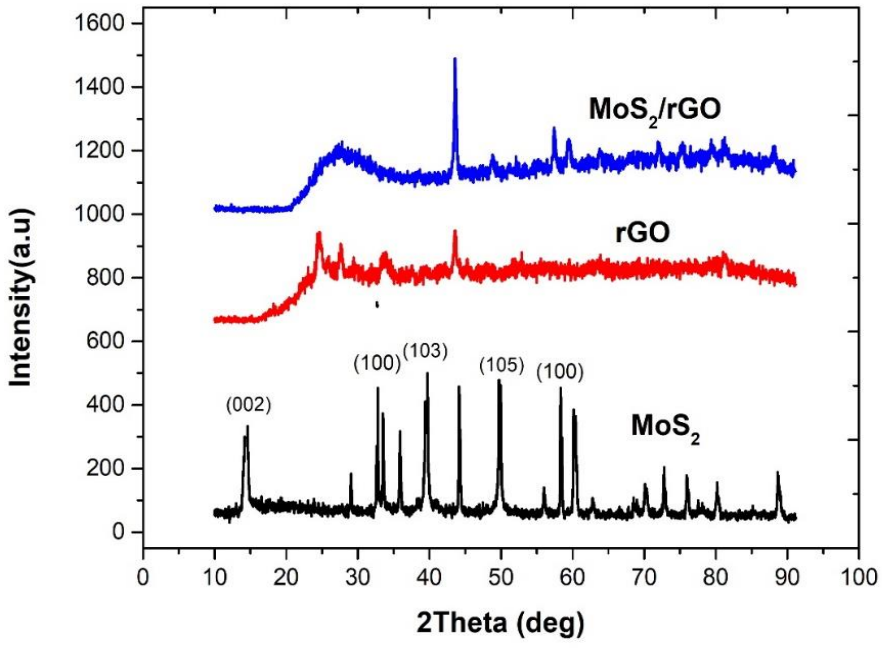

Fig 5.1 Results of XRD

5.2 Scanning electron microscopy

Pure MoS_2 film arranged by vacuum filtration was determined to be too fragile to handle given the small numbers of MoS2 sheets and weak intermolecular forces between them. **[58]** The pure MoS2 film was not freeze-dried in order to preserve its integrity; rather it was dried on a vacuum burner. The compact layer structure observed in the cross-sectional SEM image may be the product of the restacking and restructuring of 2D nanosheets during the fabrication **(Figure 5.2a**). The average pore size of the MoS2/rGO nanocomposite was 14.13 nm, which was slightly lower than the MoS2 nanocomposite's 17.69 nm (BJH analysis, Fig. **5.2c,d**). These results showed that the increased more dynamic active sites of the nanocomposites and its unique porous nanostructure would offer more surface area for the absorption of targeted atoms.

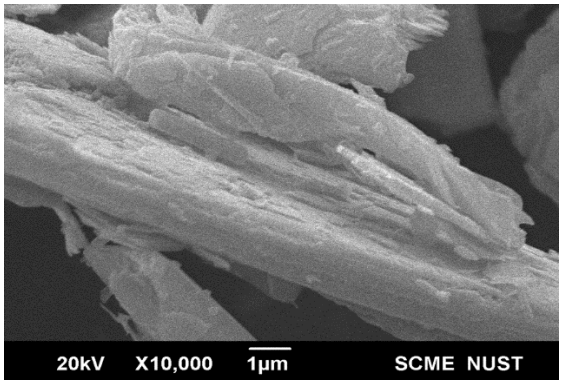

Fig 5.2 a) MoS_2

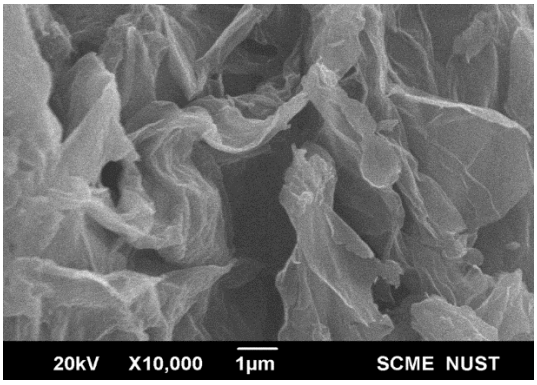

Fig 5.2 b) rGO

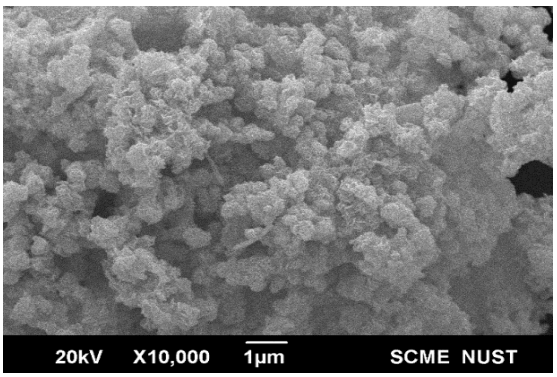

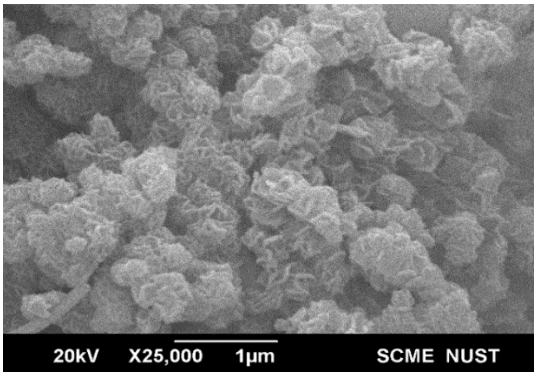

Fig 5.2 c,d) MoS_2/rGO

5.3 Fourier Transform Infra-Red (FTIR) Spectroscopy

The FTIR spectra reveal the functional groups present on MoS_2, rGO, and MoS_2/rGO nanocomposite **(Fig. 5.4).** For MoS_2 samples, the absorption bands can be seen at 1104 and 1626 cm^{-1}. The spectrum at 469 cm^{-1} is caused by the Mo-S bond, and the spectrum at 904 cm^{-1} is caused by the S-S bond. The absorption spectrum around 1104 and 1626 cm^{-1} is produced by the Mo-O vibrations and the stretching vibrations of the O-H family. The absorption spectrum at 3452 cm^{-1} is produced by the bending vibrations of O-H. The O-H absorption spectrum have been present from the undried absolute test, as evidenced by the GO spectrum's solid and broad peak at 3250-3750 cm^{-1} **[59, 60].** At 1700–1900 cm^{-1}, there is a weak signal that is comparable with COOH or C=O. The bands at 1560 and 1482 cm^{-1} serve to identify the C=C stretch of the benzyl and steroids rings, respectively. The appearance of C=C and C-O-C sp^2-hybridized was preliminarily confirmed by the peaks at 1550-1650 and 1350 cm^{-1} **[61].** The stretching of aromatic amines along the C-N and C=N axes is what is responsible for the bands at 1297 and 1237 cm^{-1}. The spectra at 1122 cm-1 reveal the in-plane bends of the benzyl C-H, whereas the spectrum at 804 cm^{-1} indicates the vibration of phenols is out-of-plane. A Tensile vibrational peak of -OH is rGO, which is located at 3373 cm^{-1}. At a wavelength of 1724 cm^{-1}, the carboxyl group of oxidized graphite exhibits the tensile vibration peak of C=O. At 1622 cm^{-1}, there are three vibration absorption peaks: epoxy C-O (1223 cm^{-1}), alkoxy C-O (1055 cm^{-1}), and the C-OH bending vibration absorption peak. In any event, the MoS_2/rGO hybrid nanostructure spectra lack a noticeable peak between 1700 and 1900 cm^{-1}, showing that the COOH and C=O compounds haven’t been observed. The Ftir analysis suggest that the graphene oxide was successfully reduced to rGO shortly after the hydrothermal reaction. Note that the rGO's excellent conductivity and strong mechanical and chemical stability can enhance the MoS_2 sonocatalytic activity **[62].**

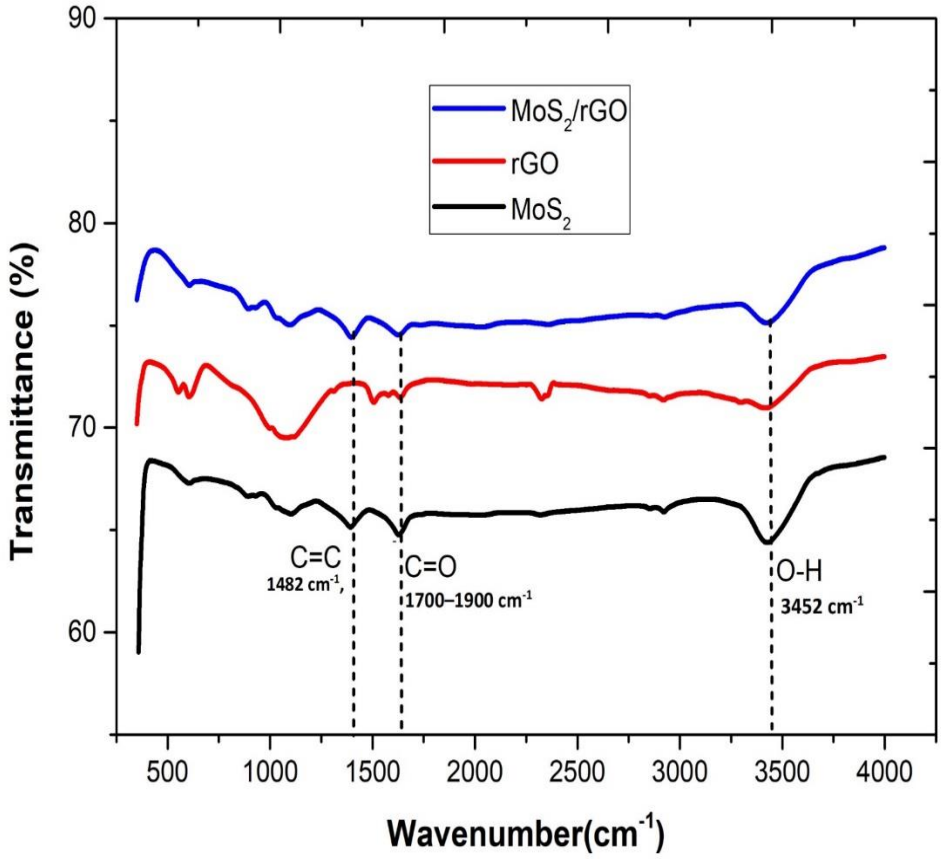

Figure 5.3 FTIR Analysis of MoS_2, rGO, MoS_2/rGO

5.4 Raman Spectroscopy

The Raman spectra of MoS_2 and a composite of MoS_2/rGO in Figure 5.4 show two different peaks. These wavenumbers around 378and 404 cm^{-1} are associated with the in-plane E^1_{2g} and out-of-plane A_{1g} vibration patterns of the MoS_2 crystal's hexagonal structure. The multilayer composition of MoS_2 is represented by the 26cm^{-1} energy value difference between them. When compared to the pure MoS_2 that is suitable for the 2H-MoS_2 phases, the peak intensities in MoS_2/rGO at 380 cm^{-1}(inner Mo-S bond vibration) and 405cm^{-1} (out-of-plane Mo-S component in Mo-S bond vibration) are quite low. The E^1_{2g} peak's lesser intensity than the A_{1g} peaks suggest that the crystalline structure of the resulting composites has significant side structures and defective sites. Their photocatalytic performance should increase as a result of this observation.

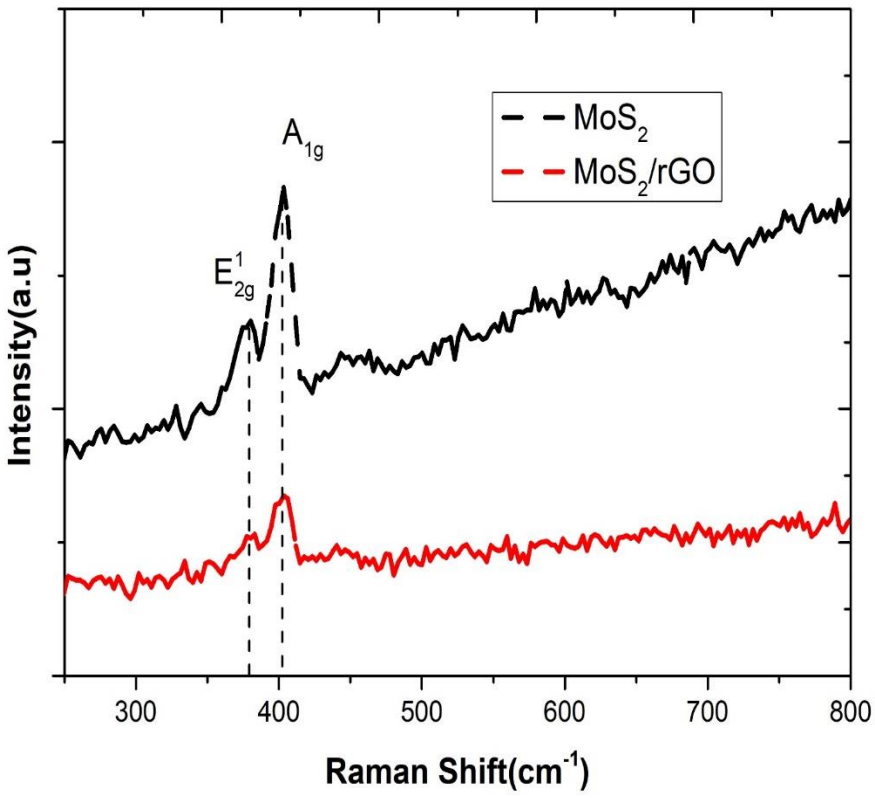

Figure 5.4 Raman Spectra

5.5 Cyclic Voltammetry (CV)

Using cyclic voltammetry, the electrochemical behavior of the UA on the MoS_2/rGO/SPE sensor was investigated (CV). On the voltammogram, the unaltered or bare electrode produces a wide and costly height. In a uric acid solution 0.2mM, 0.4 mM, 0.6mM, 0.8mM measured in 0.1M NaOH containing of UA. **[63]** Cyclic Voltammograms were recorded on a screen-printed electrode. On the bare electrode, the proscribing current density observed at -0.2 to 0.9mV potential.

Figure 5.5 In CV the electrochemical analysis of all the modified Screen printed electrode electrodes was performed in 0.1M Sodium Hydroxide (NaOH) electrolytic solution (PH = 10) containing 0.2mM Uric Acid. Figure 5.5 displays the CVs of bare SPE, MoS_2, rGO, and MoS_2/rGO@ screen printed copper-based electrode in the existence of 0.2 mM uric acid. The values of the anodic peak currents for bare SPE, MoS_2, rGO, and MoS_2/rGO@ screen printed copper-based electrode were determined to be 0.019mA, 0.055mA, 0.043mA, and 0.069mA, respectively, at potentials 0.19mV, 0.573mV, 0.33mV, and 0.542 mV. These maximum peaks readings reveal

that the MoS_2/rGO modified electrode has a peak current that is noticeably higher that the unmodified SPE. This difference may be caused by the modified electrode's increased surface region, peculiar high porosity, and adsorption rate, which allows for the accumulation of more UA on its surface.

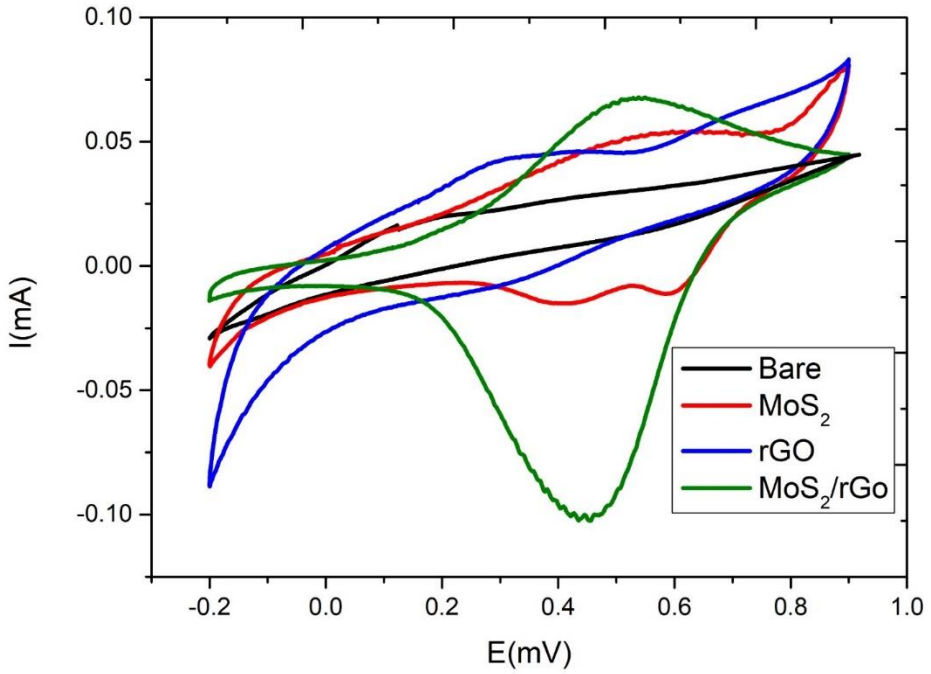

Figure 5.5 In the presence of 0.1m NaOH electrolyte and 0.2mM Uric acid (UA), cyclic voltammograms were collected at a scan rate of 100mVs^{-1} for Bare SPE, MoS_2, rGO, and MoS_2/rGO@Screen printed electrode.

Figure 5.6 The MoS_2/rGO@screen printed cupper-based electrode CV curves at various scan rates are shown in Figure 5.6, along with the linear correlation between anodic peak currents and the square root of scan rates. In the existence of 0.8mM UA, the current of anodic peaks for the MoS_2/rGO@screen printed cupper-based electrode improved as the potential scan rate increased, which also illustrates how the diffusing layer's size shrink as a consequence of the quicker scan rates (20 to 100mVs^{-1}). Higher currents are seen as a response

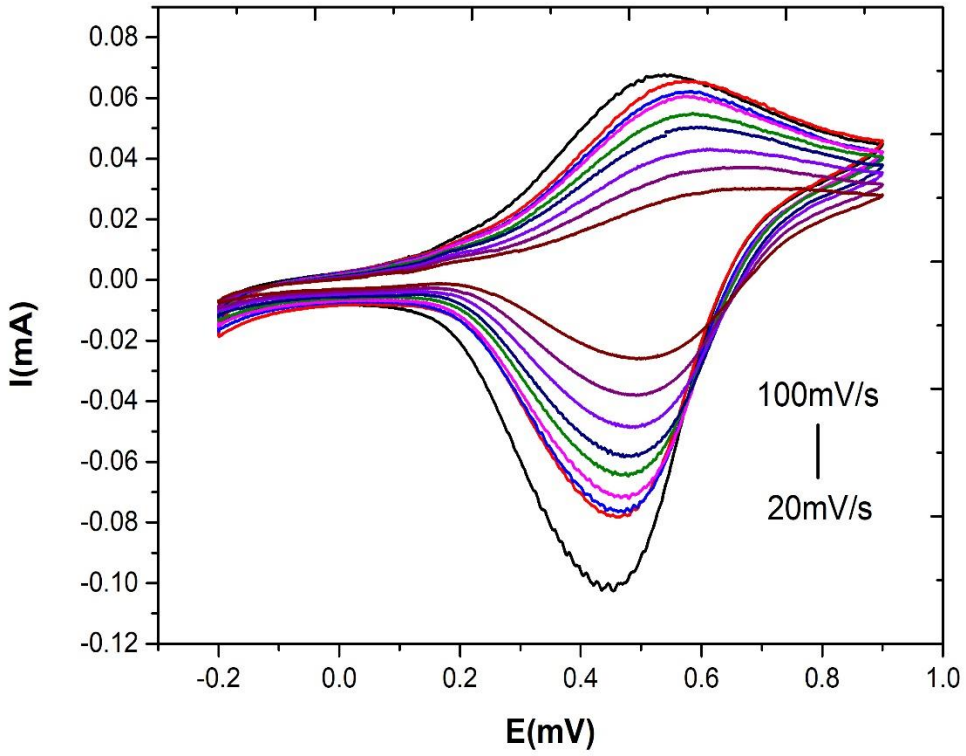

Figure 5.6 Cyclic voltammogram recorded for MoS_2/rGO nanocomposite modified SPE in 0.1M NaOH with 0.2mM uric acid (UA) at different scan rates from 20-100mVs^{-1}

The calibration curve of uric acid concentration vs current density and the CVs of MoS_2/rGO at different molar concentrations of uric acid are shown in **Figures 5.7** and **5.8**, respectively. The oxidation peak currents gradually increased as UA concentration increased as shown by the (Figure 5.7) for the MoS_2/rGO@screen printed cupper-based electrode for different UA concentrations levels ranging from 0.2mM to 0.8mM measured in 0.1M NaOH. This exhibits the MoS_2/rGO catalyst's exceptional catalytic activity in the electro-oxidation of UA. The values of the oxidation peak current derived from the CVs were plotted against various UA concentrations, as seen in (Figure5.8). The values of the oxidation peak current derived from the CVs were plotted against various UA concentrations. The linear relationship between the current and UA concentration can be determined using a calibration graph with a correlating coefficient of 0.9988. The MoS_2/rGO@screen printed cupper-based electrode electrochemical sensor showed a sensitivity of 1.03 mA mM^{-1} and limit of Detection (LOD) of 0.07mM (S/N = 3)

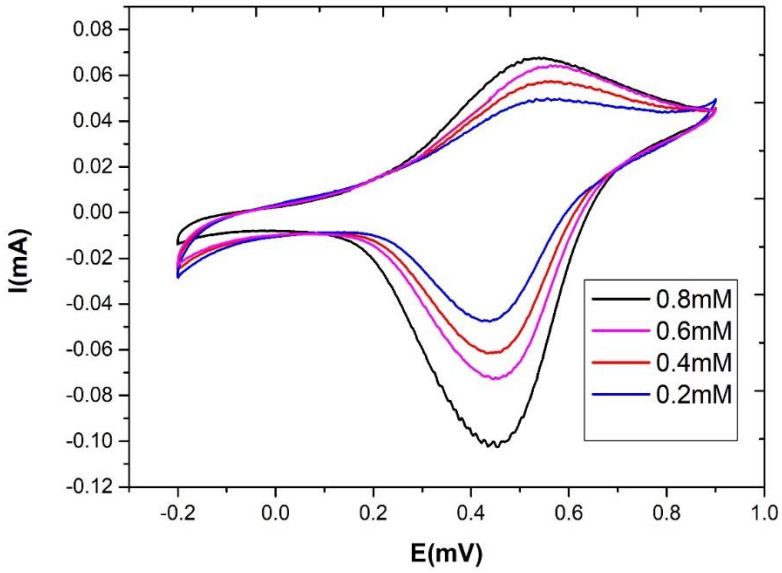

Figure 5.7 Cyclic voltammogram of MoS_2/rGO modified SPE in the presence of different concentrations of uric acid (UA) at a scan rate of 100 mVs^{-1}

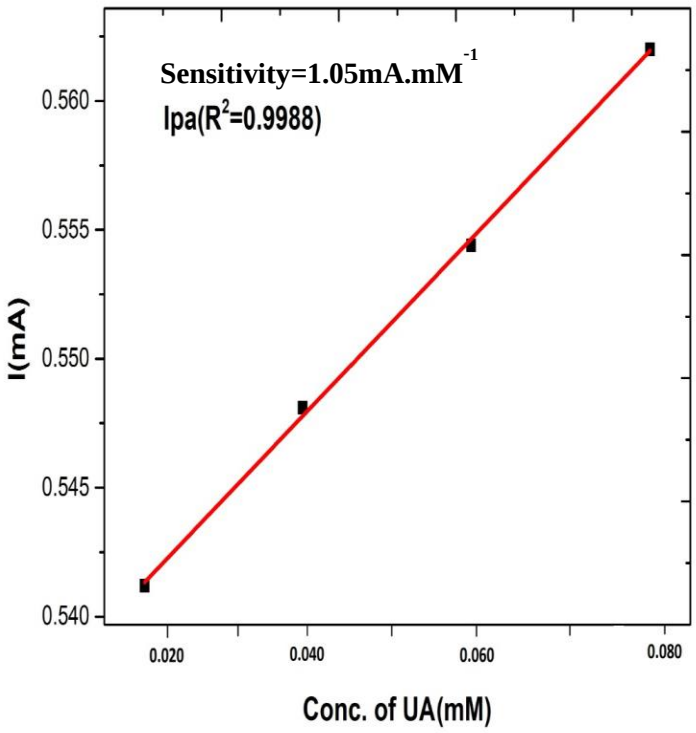

Figure 5.8 The corresponding calibration curve of current vs Uric Acid (UA) concentration.

Conclusion

In conclusion, developed a simple and efficient approach for creating a MoS_2/rGO nanocomposite with the help of Hydrothermal Methods and the characteristic of the synthesized material was confirmed through XRD, FTIR, and Raman. Fabrication of the MoS_2/rGO@Screen printed electrode copper based for electrochemical detection of Uric Acid. The nanocomposite offers a sizable accessible active surface area in addition to facilitating electron transmission. At MoS_2/rGO/SPE, a big oxidation peak at -0.2mV to 0.9mV with Ipc of about 0.06mA is obtained with a concentration of 0.8mM of UA, which is extremely larger than 0.2mM, 0.4mM, 0.6mM, concentration of UA. As we have seen when we increase the concentration of UA increase in the current density. The current of anodic peaks for MoS_2/rGO modified electrode in presence of 0.8mM UA increased with the increase in potential scan rate (20 to 100mVs^{-1}). A calibration graph with a coefficient of correlation of 0.9988 can be utilized to determine the linear connection between the current and UA concentration. The MoS_2/rGO@screen printed cupper-based electrode electrochemical sensor showed a sensitivity of 1.03 mA mM^{-1} and limit of Detection (LOD) of 0.07mM (S/N = 3). Furthermore, MoS_2/rGO nanocomposite shown strong performance for the detection of UA in samples, indicating that the suggested technique may be trustworthy and efficient for UA sensing in actual samples.

Reference

[1] Zhang, W.S.; Zhang, P.P.; Su, Z.Q.; Wei, G. Synthesis and sensor applications of MoS2 -based nanocomposites. Nanoscale 2015, 7, 18364–18378.

[2] N.A. Kumar, M.A. Dar, R. Gul, Jong-Beom Baek, Graphene and molybdenum disulphide hybrids: synthesis and applications, Mater. Today 18 (2015) 1369e7021, https://doi.org/10.1016/j.mattod.2015.01.016

[3] Xu, M.S.; Liang, T.; Shi, M.M.; Chen, H.Z. Graphene-Like Two-Dimensional Materials. Chem. Rev. 2013, 113, 3766–3798.

[4] Castro Neto, A.H.; Guinea, F.; Peres, N.M.R.; Novoselov, K.S.; Geim, A.K. The electronic properties of graphene. Rev. Mod. Phys. 2009, 81, 109–162

[5] Zhou, M.; Zhai, Y.M.; Dong, S.J. Electrochemical Sensing and Biosensing Platform Based on Chemically Reduced Graphene Oxide. Anal. Chem. 2009, 81, 5603–5613.

[6] Yu, Z.T.; Ye, J.B.; Chen, W.X.; Xu, S.R.; Huang, F.H. Fabrication of few-layer molybdenum disulfide/reduced graphene oxide hybrids with enhanced lithium storage performance through a supramolecule-mediated hydrothermal route. Carbon 2017, 114, 125–133.

[7] Yang C, Li W, Yang Z, Gu L, Yu Y. Nanoconfined antimony in sulfur and nitrogen co-doped three-dimensionally (3D) interconnected macroporous carbon for high performance sodium-ion batteries. Nano Energy. 2015;18:12-19

[8] Shao Y, Xiao J, Wang W, Engelhard M, Chen X, Nie Z, et al. Sodium ion insertion in hollow carbon nanowires for battery applications. Nano Letters. 2013;13:3909-3914

[9] Maier J. Lithium storage in carbon nanostructures. Advanced Materials. 2010;21:2664-2680

[10] Shin WH, Jeong HM, Kim BG, Kang JK, Choi JW. Nitrogen-doped multiwall carbon nanotubes for lithium storage with extremely high capacity. Nano Letters. 2012;12:2283-2288

[11] M. Molten salt activation for synthesis of porous carbon nanostructures and carbon sheets. Carbon. 2014;69:460-466

[12] Wang J, Kaskel S. KOH activation of carbon-based materials for energy storage. Journal of Materials Chemistry. 2012;22:3710-23725

[13] Wang S, Xiao C, Xing Y, Xu H, Zhang S. Carbon nanofibers/nanosheets hybrid derived from cornstalks as a sustainable anode for Li-ion batteries. Journal of Materials Chemistry A. 2015;3:6742-6746

[14] Abdel Salam M, Mokhtar M, Basahel SN, Al Thabaiti SA, Obaid AY. Removal of chlorophenol from aqueous solution by multi-walled carbon nanotubes: Kinetic and thermodynamic studies. Journal of Alloys and Compounds. 2010;500:87-92

[15] Al-Johani H, Abdel Salam M. Kinetics and thermodynamic study of aniline adsorption by multi-walled carbon nanotubes from aqueous solution. Journal of Colloid and Interface Science. 2011;360:760-767

[16] Xin X, Wei Q , Yang J, Yan L, Feng R, Chen G, et al. Highly efficient removal of heavy metal ions by aminefunctionalized mesoporous Fe3O4 nanoparticles. Chemical Engineering Journal. 2012;184:132-140

[17] Khandoker N, Hawkins SC, Ibrahim R, Huynh CP, Deng F. Tensile strength of spinnable multiwall carbon nanotubes. Procedia Engineering. 2011;10:2572-2578

[18] Fam DWH, Palaniappan A, Tok AIY, Liedberg B, Moochhala SM. A review on technological aspects influencing commercialization of carbon nanotube sensors. 2011;157:1-7 Fam DWH, Palaniappan A, Tok AIY, Liedberg B, Moochhala SM. A review on technological aspects influencing commercialization of carbon nanotube sensors. 2011;157:1-7

[19] Novoselov, K.S., Geim, A.K., Morozov, S.V., et al., Electric Field Effect in Atomically Thin Carbon Films, Science, 2004, vol. 306, no. 5696, pp. 666–669.

[20] Tkachev, S.V., Buslaeva, E.Yu., and Gubin, S.P., Graphene: A Novel Carbon Nanomaterial, Inorg. Mater., 2011, vol. 47, no. 1, pp. 1–10.

[21] Geim, A.K. and Novoselov, K.S., The Rise of Graphene, nat. mater, 2007, vol 6, no 3

[22] Gubin, S.P. and Tkachev, S.V., Grafen i rodstvennye nanoformy ugleroda (Graphene and Related carbon nanomaterials) Moscow. Librokom 2012

[23] Hummers, W.S. and Offeman, R.E., Preparation of Graphitic Oxide, J. Am. Chem. Soc., 1958, vol. 80, no. 6, pp. 1339–1339.

[24] Zhang, W.S.; Zhang, P.P.; Su, Z.Q.; Wei, G. Synthesis and sensor applications of MoS2 -based nanocomposites. Nanoscale 2015, 7, 18364–18378

[25] Wang, Y.S.; Ma, T.C.; Ma, S.Y.; Liu, Y.J.; Tian, Y.P.; Wang, R.N.; Jiang, Y.B.; Hou, D.J.; Wang, J.L. Fluorometric determination of the antibiotic kanamycin by aptamer-induced FRET quenching and recovery between MoS2 nanosheets and carbon dots. Microchim. Acta 2017, 184, 203–210.

[26] Facile in situ fabrication of rGO/MoS2 heterostructure decorated with gold nanoparticles with enhanced photoelectrochemical performance

[27] L. Chen, F. He, N. Zhao, R. Guo, Fabrication of 3D quasi-hierarchical Z-scheme RGO-Fe2O3-MoS2 nanoheterostructures for highly enhanced visible-light-driven photocatalytic degradation, Appl. Surf. Sci. 420 (2017) 669–680, https://doi.org/ 10.1016/j.apsusc.2017.05.099.

[28] A.P. Nayak, S. Bhattacharyya, J. Zhu, J. Liu, X. Wu, T. Pandey, C. Jin, A.K. Singh, D. Akinwande, J.F. Lin, Pressure-induced semiconducting to metallic transition in multilayered molybdenum disulphide, Nat. Commun. 5 (2014) 1–9. **https://doi.org/10.1038/ncomms4731**.

[29] R. Kappera, D. Voiry, S.E. Yalcin, B. Branch, G. Gupta, A.D. Mohite, M. Chhowalla, Phase-engineered low-resistance contacts for ultrathin MoS2 transistors, Nat. Mater. 13 (2014) 1128–1134. **https://doi.org/10.1038/nmat4080**.

[30] K. Chang, W. Chen, L-cysteine-assisted synthesis of layered MoS2/graphene composites with excellent electrochemical performances for lithium-ion batteries, ACS Nano 5 (2011) 4720–4728

[31] L. Liao, J. Zhu, X. Bian, L. Zhu, M.D. Scanlon, H.H. Girault, B. Liu, MoS2 formed on mesoporous graphene as a highly active catalyst for hydrogen evolution, Adv. Funct. Mater. 23 (2013) 5326–5333.

[32] L. Liao, J. Zhu, X. Bian, L. Zhu, M.D. Scanlon, H.H. Girault, B. Liu, MoS2 formed on mesoporous graphene as a highly active catalyst for hydrogen evolution, Adv. Funct. Mater. 23 (2013) 5326–5333.

[33] D. Zhu, W. Liu, D. Zhao, Q. Hao, J. Li, J. Huang, J. Shi, J. Chao, S. Su, L. Wang, Labelfree electrochemical sensing platform for microRNA-21 detection using thionine and gold nanoparticles co-functionalized MoS2 nanosheet, ACS Appl. Mater. Interfaces 9 (2017) 35597–35603.

[34] M. Acerce, D. Voiry, M. Chhowalla, Metallic 1T phase MoS2 nanosheets as supercapacitor electrode materials, Nat. Nanotechnol. 10 (2015) 313–318.

[35] K. Chang, W. Chen, L-cysteine-assisted synthesis of layered MoS2/graphene composites with excellent electrochemical performances for lithium-ion batteries, ACS Nano 5 (2011) 4720–4728

[36] B. Radisavljevic, A. Radenovic, J. Brivio, V. Giacometti, A. Kis, Single-layer MoS2 transistors, Nat. Nanotechnol. 6 (2011) 147–150

[37] P. Jing, H. Yi, S. Xue, Y. Chai, R. Yuan, W. Xu, A sensitive electrochemical aptasensor based on palladium nanoparticles decorated graphene-molybdenum disulfide flowerlike nanocomposites and enzymatic signal amplification, Anal. Chim. Acta 853 (2015) 234–241.

[38] W.S. Hummers, R.E. Offeman, Preparation of graphitic oxide, J. Am. Chem. Soc. (1958) 1339

[39] Y. Guo, S. Guo, J. Ren, Y. Zhai, S. Dong, E. Wang, Cyclodextrin functionalized graphene nanosheets with high supramolecular recognition capability: synthesis and host guest inclusion for enhanced electrochemical performance, Nanoscale 4 (2010) 4001–4010.

[40] One-pot synthesized AuNPs/MoS2/rGO nanocomposite as sensitive electrochemical aptasensing platform for nucleolin detection

[41] J. Yang, C. Zang, L. Sun, N. Zhao, X. Cheng, Synthesis of graphene/Ag nanocomposite with good dispersibility and electroconductibility via the solvothermal method, Mater. Chem. Phys. 129 (2011) 270–274.

[42] L. Chen, X. Wang, X. Zhang, H. Zhang, 3D porous and redox-active Prussian blue-ingraphene aerogels for highly efficient electrochemical detection of H2O2, J. Mater. Chem. 22 (2012) 22090–22096.

[43] L. Tian, L. Liu, Y. Li, Q. Wei, W. Cao, 3D sandwich-type prostate-specific antigen (PSA) immunosensor based on rGO-MWCNT-Pd nanocomposite, New J. Chem. 39 (2015) 5522–5528

[44] F.Y. Ban, S. Jayabal, N.L. Hong, H.W. Lee, N.M. Huang, Synthesis of nitrogen-doped reduced graphene oxide-multiwalled carbon nanotube composite on nickel foam as an electrode for high-performance supercapacitor, Ceram. Int. 43 (2016) 20–27.

[45] Copper-based ternary metal sulfide nanocrystals embedded in graphene oxide as photocatalyst in water treatment Olalekan C. Olatunde, Damian C. Onwudiwe,

[46] The application of graphene oxide as a corrosion barrier Iman Khosravi, ... Mahdi Yeganeh, in Corrosion Protection at the Nanoscale, 2020

[47] J.R. Lince, Tribology of Co-sputtered nanocomposite Au/MoS2 solid lubricant films over a wide contact stress range, Tribol. Lett. 17 (2004) 419–428

[48] Zh. Chen, H. Yan, T. Liu, S. Niu, Nanosheets of MoS2 and reduced graphene oxide as hybrid fillers improved the mechanical and tribological properties of bismaleimide composites, Compos. Sci. Technol. 125 (2016) 47–54

[49] Q. Wan, Y. Jin, P. Sun, Y. Ding, Rheological and tribological behaviour of lubricating oils containing platelet MoS2 nanoparticles, J. Nanoparticle Research 16 (2014) 2386–2386.

[50] M. Chhowalla, G.A.J. Amaratunga, Thin film soffullerene-like MoS2 nanoparticles with ultra-low frictionand wear, Nature 407 (2000)

[51] Y. Areerob, J.Y. Cho, W.K. Jang, W.C. Oh, Enhanced sonocatalytic degradation of organic dyes from aqueous solutions by novel synthesis of mesoporous Fe3O4-graphene/ZnO@SiO2 nanocomposites, Ultrasonics Sonochemistry 41 (2018) 267

[52] L.L. Tan, W.J. Ong, S.P. Chai, B.T. Goh, A.R. Mohamed, Visible-light-active oxygen-rich TiO 2 decorated 2D graphene oxide with enhanced photocatalytic activity toward carbon dioxide reduction, Applied Catalysis B Environmental 179 (2015) 160-170.

[53] M. Acik, G. Lee, C. Mattevi, M. Chhowalla, K. Cho, Y.J. Chabal, Unusual infrared-absorption mechanism in thermally reduced graphene oxide, Nature Materials 9 (10) (2010) 840-845

[54] N. Z, L. L, L. Zhang, Q. Shao, Z. W, C. X, X. S, A universal strategy to prepare functional porous graphene hybrid architectures, Advanced Materials 26 (22) (2014) 3681-3687.

[55] Enujekwu Francis M., Zhang Yue, Ezeh Collins I., Zhao Haitao, Xu Mengxia, Besley Elena, George Michael W., Besley Nicholas A., Do Hainam, Wu Tao. N-doping enabled defect-engineering of MoS2 for enhanced and selective adsorption of CO2: A DFT approach [J]. Applied Surface Science, 2021, 542.

[56] Hongxia W., Diana T., Jun Q., Fuyuan D., Dusan L. Supercapacitors: MoS2/Graphene Composites as Promising Materials for Energy Storage and Conversion Applications [J]. Advanced Materials Interfaces, 2019, 6.

[57] Kumar R., Dias W., Rubira R. J. G. et al. Simple and Fast Approach for Synthesis of Reduced Graphene Oxide–MoS2 Hybrids for Room Temperature Gas Detection [J]. IEEE Transactions on Electron Devices, 2018, 65(9): 3943-3949

[58] Wu Z. S., Zhou G., Yin L. C. et al. Graphene/metal oxide composite electrode materials for energy storage [J]. Nano Energy, 2012, 1(1): 107-131.

[59] Ji L., Rao M., Zheng H. et al. Graphene Oxide as a Sulfur Immobilizer in High Performance Lithium/Sulfur Cells [J]. Journal of the American Chemical Society, 2011, 133 (46): 18522-18525.

[60] Cao X., Shi Y., Shi W. et al. Preparation of MoS2- coated three-dimensional graphene networks for high-performance anode material in lithium-ion batteries [J]. small, 2013, 9 (20): 3433-3438.

[61] Wang Z., Chen T., Chen W. et al. CTAB-assisted synthesis of single-layer MoS2-graphene composites as anode materials of Li-ion batteries [J]. Journal of Materials Chemistry A, 2013, 1 (6): 2202-2210.

[62] Kanjun S., Kanjun S., Guohong Z., guangming M. Electrochemical behavior of phenol on glassy carbon electrode [J]. Gansu science and technology, 2014 (01): 23-25.

[63] Li H., Yin Z., He Q. et al. Fabrication of Single- and Multilayer MoS2 Film-Based Field-Effect Transistors for Sensing NO at Room Temperature [J]. Small, 2012, 8 (1): 63-67.